Jorge Miguel Ribeiro Martins

Mestre em Engenharia Mecânica

Joining Copper to Stainless Steel by Friction Stir Diffusion Process

Dissertação para obtenção do Grau de Mestre em Engenharia Mecânica

Orientadora: Prof.ª Doutora Rosa Maria Mendes Miranda, Professora Associada com Agregação, FCT/UNL

Co-orientador: Prof. Doutor Pedro Miguel dos Santos Vilaça da Silva, Professor Auxiliar, UTL/IST

Júri:

Presidente: Prof. Doutor Jorge Joaquim Pamies Teixeira
Arguente: Prof.ª Doutor(a) Maria Luísa Coutinho Gomes de Almeida Quintino
Vogal: Prof.ª Doutor(a) Rosa Maria Mendes Miranda
Vogal: Prof. Doutor Pedro Miguel dos Santos Vilaça da Silva

FACULDADE DE CIÊNCIAS E TECNOLOGIA
UNIVERSIDADE NOVA DE LISBOA

Julho de 2013

Joining Copper to Stainless Steel by Friction Stir Diffusion Process

Nota: A presente dissertação foi redigida segundo a ortografia anterior ao novo acordo ortográfico.

Jorge Miguel Ribeiro Martins

Mestre em Engenharia Mecânica

Joining Copper to Stainless Steel by Friction Stir Diffusion Process

Dissertação apresentada na Faculdade de Ciências e Tecnologia da Universidade Nova de Lisboa para obtenção do Grau de Mestre em Engenharia Mecânica

Julho 2013

Agradecimentos

Gostaria de agradecer à minha orientadora, Professora Rosa Maria Mendes Miranda, por me integrar num projecto inovador, pelo interesse demonstrado, empenho e tempo investidos, bem como as sugestões de melhoria na revisão deste trabalho.

Ao meu co-orientador Professor Pedro Miguel dos Santos Vilaça da Silva um sincero obrigado pela sua disponibilidade, interesse pelo projeto, ideias e equipamento que em muito contribuíram para a qualidade do trabalho desenvolvido.

O meu profundo obrigado ao Mestre João Pedro Machado da Gandra pela sua amizade e apoio, bem como a sua total disponibilidade, conhecimento e empenho que me doou ao longo deste curso e trabalho de investigação.

O meu agradecimento ao Professor Rui Jorge Cordeiro Silva pela ajuda nos ensaios SEM/EDS bem como ao Professor Alexandre José da Costa Velhinho na utilização do equipamento de microscópia óptica.

Ao Sr. António Campos e Sr. Paulo Magalhães um especial obrigado pela sua amizade e assistência técnica.

Ao colega João Prior e Mestre Filipe Nascimento o meu agradecimento por toda a ajuda prestada durante o trabalho experimental decorrido na STM-IST, em especial pelo apoio e amizade.

Ao Mestre João Pedro Oliveira o meu obrigado pela ajuda e tempo dispensado na utilização do equipamento de ensaios de corte e flexão.

O autor reconhece a enorme importância do financiamento suportado pela Fundação para a Ciência e Tecnologia para o projeto “Desenvolvimento da tecnologia de processamento por fricção linear para produzir materiais com gradiente de funcionalidade e melhoria de superfícies para aplicações avançadas de engenharia – FRISURF”, assim como o fornecimento de material provido da empresa Siemens S.A.

Agradecimento aos colegas de laboratório do Núcleo de Tecnologia Industrial do Departamento de Engenharia Mecânica da FCT, pela cooperação e apoio recíproco.

A todos os meus colegas, em particular a Júlio Balagões, Rodrigo Roçadas, Duarte Silva, Vasco Sobral, Guilherme Viegas, João Alves, André Bandeira que me acompanharam durante o curso e especialmente no desenvolvimento deste projeto, um profundo agradecimento pela amizade e cooperação.

A todos os meus amigos que sempre se fazem presentes com o seu apoio e gratuidade. Um especial obrigado ao António Vieira e Filipe Brás pela revisão do texto.

À Isabel pelo carinho, compreensão e incentivo demonstrados em cada momento.

À minha família pela compreensão e apoio, em particular a Guilhermino Lima Martins, meu pai, pelos sacrifícios que fez e condições que sempre me proporcionou, um profundo obrigado.

Acknowledgements

I would like to thank my supervisor, Professor Rosa Maria Mendes Miranda, for integrating me into an innovative project, for the interest, commitment and time invested, as well as suggestions for improvement in reviewing this work.

To my co-supervisor Professor Pedro Miguel dos Santos da Silva Vilaça a sincere thanks for your availability, interest in the project, ideas and equipment that contributed greatly to the quality of the work.

My honest thank to Master João Pedro Machado Gandra for your friendship and support, as well as your full availability, knowledge and effort that you gave me throughout this course and research work.

My thanks to Professor Rui Jorge Cordeiro Silva for the help provided in SEM / EDS testing and to Professor Alexandre José da Costa Velhinho the use of optical microscopy equipment.

To Mr. António Campos and Mr. Paulo Magalhães, one particular thanks for their friendship and assistance.

To my colleague João Prior and Master Filipe Nascimento, my thanks for all the help provided during the experimental work elapsed in STM-IST, especially for the support and friendship.

To Master João Oliveira my thanks for your help and time spent for the use of equipment to shear and bending tests.

The author recognizes the great importance of funding by the Foundation for Science and Technology for the project "Technology developments of Friction stir processing to produce functionally graded materials and improve surfaces for advanced engineering applications - FRISURF", as well as the supply of material supplied from Siemens S.A.

An appreciation to my colleagues of laboratory at the Center for Industrial Technology Department of Mechanical Engineering, FCT, cooperation and reciprocal support.

To all my colleagues, particularly Julio Balagões, Rodrigo Roçadas, Duarte Silva, Vasco Sobral, Guilherme Viegas, João Alves, André Bandeira that accompanied me during the course and especially in the development of this project, a deep appreciation for the friendship and cooperation.

To all my friends who are always present with their support and generosity. A special thank to António Vieira and Filipe Brás for reviewing the text.

A special thank you to Isabel for caring, understanding and encouragement demonstrated in every moment.

Finally to my family for their understanding and support, namely Guilhermino Lima Martins, my father, for the sacrifices that have been made and conditions that were provided, a heartfelt thanks.

Sumário

Uma das principais tendências em soldadura e tecnologias de ligação reside na junção de materiais dissimilares tirando partido das propriedades de cada material individualmente.

A ligação cobre com aço inoxidável destaca-se apresentando aplicações industriais cruciais, onde a título de exemplo, são requeridos os valores mais altos de condutividades elétricas e térmicas associados a materiais com boa resistência à corrosão. Contudo, a junção destes materiais suscita dificuldades, devido à diferente composição química e propriedades termofísicas. Além disso, estes materiais formam facilmente fases intermetálicas que reduzem a resistência mecânica da ligação. Assim, investigar a viabilidade de aplicação de tecnologias de processamento alternativas assume um papel relevante.

Os processos de ligação no estado sólido têm sido alvos de investigação para esta aplicação, nomeadamente a soldadura por fricção linear. Recentemente, tem sido explorada uma variante deste processo, onde a difusão local é o mecanismo fundamental de ligação acionado por fricção linear. A vantagem do processo de difusão por fricção linear é o efeito prejudicial mínimo observado em ambos metais, prevenindo os problemas identificados.

Como este processo não se encontra completamente desenvolvido, a presente tese tem como objetivo estudar o processo de difusão por fricção linear (PDFL) para ligar o cobre ao aço inoxidável. Foram produzidas juntas sobrepostas alterando parâmetros de processamento como rotação, velocidade de deslocamento e força de forjamento. Foi estudado o efeito dos parâmetros de processamento sobre a largura da ligação efetiva, assim como a caraterização das juntas relativamente às propriedades de resistência mecânicas e características microestruturais na interface.

As condições termomecânicas e o tempo durante o PDFL resultaram em uma interface com difusão entre os dois materiais inferior a 3 μm. A resistência ao corte das juntas sobrepostas depende da espessura do material envolvido, no entanto foi atingida uma eficiência de ligação até 73,8%.

Palavras chave

Soldadura por fricção linear

Soldadura por difusão

Cobre

Aço Inoxidável

Ligação dissimilar

Resistência mecânica

Abstract

One of the major trends in welding and joining technology is to join dissimilar materials taking advantage of individual materials properties.

Among these, copper to stainless steel joining has significant industrial applications and importance where e.g. the highest electrical and thermal conductivities are required to engineering materials associated to good corrosion resistance. However, joining these materials is difficult due to their very different chemical composition and thermo-physical properties. Additionally, they easily form intermetallic phases that deteriorate the mechanical strength of the joint. Thus investigating the feasibility of applying alternative processing technologies is relevant.

Solid state processes have been investigated for this application, namely friction stir welding. Recently, a variant has been exploited where local diffusion is the fundamental joining mechanism triggered by friction stir. The advantage of friction stir diffusion process is the minimal detrimental effect on both materials, preventing some critical identified problems.

Since this process is not well developed, this thesis aimed to study friction stir diffusion process (FSDP) to join copper to stainless steel. Lap joints were produced varying processing parameters, namely, rotation and travel speeds and axial forging force. The effect of processing parameters on the width of effective joining was studied, as well the joints characterization for mechanical resistance properties and microstructural features at the interface.

The thermo-mechanical conditions and time during the FSDP resulted in an interface with diffusion between both materials below 3 μm. The shear strength of the lap joints depends on the material thickness involved, but joining efficiencies up to 73.8 % were achieved.

Keywords

Friction stir welding

Diffusion process

Copper

Stainless steel

Dissimilar joint

Mechanical resistance

Index

Table Index

Figure Index

Abbreviations and Symbols

AS	Advancing side
BM	Base material
BSE	Back-scsttered electron
Df	Downward force
d_{probe}	Probe diameter
EC_l	Energy comsumption per unit of length
EDS	Energy dispersive spectroscopy
fb	Free of burr
FCT-UNL	Faculdade de Ciências e Tecnologia - Universidade Nova de Lisboa
FSDP	Friction stir diffusion process
FSW	Friction stir welding
F_x	Force applied in the X direction
HAZ	Heat affected zone
IMC	Intermetallic compound
IST-UTL	Instituto Superior Técnico - Universidade Técnica de Lisboa
l	Distance between probe centers in two successive steps
$l_{processed}$	Processed length by the tool
NtEZ	Near to edge zone
OR	Overlapping ratio
P_e	Mechanical power provided by equipment
RS	Retreating side
SE	Secondary electrons
SEM	Scanning electron microscopy
SZ	Stationary zone
t	Time of processing
TMAZ	Thermo-mechanically affected zone
TWI	The welding institute

T_z	Binary in the Z-axis
ϑx	Travel speed
wb	Burr formation
Ω	Rotation speed

1. Introduction

1.1. Motivation

An important challenge in the design and processing of engineering materials is to combine incompatible properties of materials in the same component [1,2]. This possibility can be used to reduce weight in applications such as aerospace and automotive industries or for corrosion resistant components in petrochemical industry. As traditional fusion welding processes have difficulty to produce good overlapped welds in dissimilar materials, due to the differences in melting points and thermo physical properties such as the thermal diffusion and linear thermal expansion coefficients, solid state processes present advantages in terms of metallurgical compatibility and soundness of the joints.

Joining processes involving dissimilar materials are been developed for two main situations:

- For surface cladding aiming to improve wear and corrosion resistance, in industrial applications where surface properties are the main requirement.
- In joining dissimilar materials for applications where combination of mechanical and structural proprieties are request.

The former involve mostly lap joint configuration while the second is not limited to this one but can involve other types of joints.

Solid state welding is being increasingly used for joining dissimilar metals (i.e. bimetals) rather than fusion welding. It is justified by the absence of melting faces of parent metals and metallurgical changes of the joints are minimized [3]. Joining is achieved by diffusion controlled mechanism. One of the most common processes for joining dissimilar materials is brazing, with the disadvantage of a poor resistance of the joints in service at high temperatures. Therefore, diffusion bonding is proposed as the best-suited alternative bonding process [2]. However, the dissemination of this processes requires more complex equipment and long processing time, and therefore, it becomes often unattractive for the industrials [4].

Nowadays, manufacturing technology requires a joining process that is versatile at both high temperatures and low pressures, in order to avoid unwanted phase transformations and large deformation but also a better efficiency of materials [5]. Therefore, it is clear that the challenge is the development of reliable and cost effective joining methods without neglecting the environment [1].

The success of this joining method would be interesting for industries applying Cu and SS as in energy generation as nuclear power plants or in chemical industries.

1.2. Objectives

The main aim of this thesis is to join copper to stainless steel in lap joints by Friction Stir Diffusion Process (FSDP) minimizing or even avoiding the problems that occur in dissimilar joining by fusion processes, namely: formation of intermetallic compounds, structural changes, phase transformations, that reduce the mechanical resistance of the joints.

Friction Stir Diffusion Process allows to diffusion-join dissimilar materials based on a lap-welding plate configuration. The cladding material in plate form is pre-positioned on top of the substrate. Then, a non-consumable tool comprising a probe and a shoulder is used to friction stir process the cladding material. Although the probe does not penetrate the substrate, heat and pressure given by the FSDP of the cladding material will promote a diffusion joining at the interface soundly bonding the assembly.

Tests were performed using a FSW equipment available at IDMEC. The influence on the surfaces processed were assessed by several techniques of materials characterization namely, optical and scanning electron microscopy, hardness tests, shear tests and bending tests. The surfaces processed were characterized in order to establish the best processing strategy for surface improvement in manufacturing.

1.3. Structure

This thesis is structured in five chapters.

Chapter 2 highlights the state of the art, which provides a theoretical framework that will support the interpretation of results in future dissertation. This section is comprised of an approach to industrial relevance of steel-copper joints, their technological difficulties and bonding processes. This last point is addressed with some usual coating methods such as laser cladding, hot isostatic pressure, explosion cladding, diffusion bonding and the recent friction stir diffusion process.

Chapter 3 describes the experimental set-up, addressing the materials characterization, FSDP equipment, work methodology and characterization techniques used in the analysis of the surface.

Chapter 4 presents the results and discussion of the processing. This section consists of four main themes, including the analysis of the base material, metallurgical characterization, mechanical characterization and energy consumption.

Chapter 5 reports the final conclusions and suggestions for future work for improving the FSDP on lap joints.

2. State of the art

2.1. Industrial relevance of bimetals Cu / Ss

The demand for copper-steel connection has increased due to the advantages of this bimetal. Copper has an excellent thermal and electrical conductivity, and good deformability. On the other hand, stainless steel provides excellent wear resistance, high strength, toughness and resistance to corrosion. The interest for bimetals is high because they provide the best of the two metals at low cost. This articulation is beneficial in industrial applications such as: automotive, railways, naval, aviation, aerospace, chemical and metallurgical equipment. Examples are:

- Production of parts for smelting furnaces can rise the reliability and service life of equipment [6], reducing the consumption of resources and energy.
- Cooling channels in injection moulding [7]. It has been reported the manufacture of turbine wheels with these materials diffusion bonding [8].
- Nuclear environments of light water and fast breeder reactors to improve heat conduction in some areas of the divertor [9].

2.2. Technological challenges

Usually, diffusion bonding of dissimilar materials originates poor mechanical properties, due to the residual stress generated by the differences in the expansion coefficient, compression strength and thermal conductivity of individual materials. This can lead to the creation and propagation of micro voids and micro cracks in the interface, decreasing the strength of the joint [10]. Distortion, inclusions and segregation defects are found and in order to minimize this problem, the joining may be done with a compatible layer [2]. In the case of connections of stainless steel-copper, layers of nickel are commonly used, due to its transient nature, corrosion resistance at high temperatures and good solubility. Other interlayers have also been reported such as tin-bronze (TB), Au, and TB Combined Au [11].

2.3. Joining processes

Some of the most relevant cladding processes are: laser, hot isostatic pressure, explosion and diffusion welding.

Several authors [3, 4, 12], reported that solid state processes constitute suitable alternatives for producing dissimilar metal joints, because the melting temperature of the base materials is not achieved. Therefore, the defects, the structural damage and the heat-affected zone can be minimized. Even so, melting processes are still widely used.

2.3.1. **Laser cladding/alloying**

Laser coating has been largely used to modify surface properties [13]. However, multi-stage processes increase the processing time [7]. In these methods using powder or wire from two more feeders, the same or dissimilar materials are conveyed using an inert gas stream. Simultaneously, the laser irradiates a substrate surface creating a small melt pool. The combination of these movements gives rise to a well-bonded solid clad [7, 13]. Laser joining with copper showed some disadvantages as the formation of intermetallics or the high reflectivity of copper to laser light, thus, there are not so many studies on laser cladding involving copper. Even so, the introduction of an interlayer may overcome some of the problems [14].

Syed et al [7] produced a surface coating on steel with copper powder and nickel wire. The hardness tests showed a range of clad mean hardness between 108 - 600 HV depending on the feeding rates of copper and nickel. These factors also impacted the thermal conductivity and diffusivity of the specimen. The solidification front temperature was of 1000 - 1400 ºC, sufficient to melt the copper particles, but lower than iron and nickel melting points. The same authors [13] showed some analysis with discontinuities and lack of homogeneity for copper and nickel powders on H13 steel, due to the differences of the materials melting temperatures and to the low mass flow rate of nickel powder. Upon solidification of the molten pool, only the cooper was melted. These results showed the copper-rich thin layer on top of the clad (more than 90 %), while the copper wire and nickel powder had concentrations of 78 to 82 % Cu.

2.3.2. **Hot isostatic pressure**

Hot isostatic pressure is one of most advanced diffusion bonding technologies [15]. It is used to process powder or solid materials under the action of high inert gas pressures (up to 200 MPa), at high temperatures (up to 2000 °C) and it is often combined with heat treatment of bonded structure [16, 17]. The treatment effectively refines the grain structure, removes porosity and micro-defects, therefore, increasing the strength joint. This method requires time and some complexity. Polishing or machining is required to prepare flat surface, clean surface free from grease, drying under air and other operations [16, 18].

The CuCrZr/SS 316LN joints with interlayer (Fe42Ni) produced by LeMarois et al [19], fractured and plastically deformed in the Cu alloy. For dispersion strengthened Cu/SS 316 bonding, the tensile tests of joints fractured in the base metal of copper or in the interface [15]. Afterwards, Ivanov et al [16] reported that, for the previous materials join, it is advisable to use temperatures of 920 - 1050 ºC, pressures of 120 - 140 MPa for 1 to 4 hours. Furthermore, it was possible to produce stronger joints than 90% tensile strength base metal DS Cu and CuCrZr alloys. Goods and Puskar [18] presented results of yield strengths of 103 MPa at bonding temperatures of 1040 ºC. After the heat treatment at 560 ºC, the yield strength rised to 225 MPa, higher than that of the base alloy CuCrZr. However, due to high temperatures, the grain size of cooper alloy was very coarse and variable in size.

2.3.3. **Explosive cladding**

Explosive joining is a solid state process that joins two plates through the oblique high velocity collision. It is possible a strong bond between two materials with good physical and metallurgical properties of the bonded region. The main parameters used are: the angle of inclination, the detonation velocity and the flyer plate thickness [20]. This technology has the particular characteristic of generating a surface clean of contaminants, as the plates move along the interface and it is especially recommended for joining large areas [18, 21]. However, explosion bonding can require vacuum chambers or other forms to protect the operator. Addicionally, it is limited by flexibility, noise and sound vibrations [21].

Joining interface can show three morphologies, depending on the angle and velocity of impact: wavy, flat and melted layer (Figure 2.1) [21].

Durgutlu et al. [22] reported bonding of pure copper to stainless steel without defects, melting voids or intermetallic compounds, on the interface. The microstructures presented on interface, elongated grains in the explosive direction, straight and waviness morphologies (Figure 2.1). Wavy layers had a increase of bond surface area and also higher strength [21]. Hardness of surfaces was superior after explosion due to the deformation hardening caused by collision on the surface. Goods and Puskar [18] showed results of yield strengths up to 300 MPa (after an heat treatment at 560 ºC), higher than the base material of alloy CuCrZr. Residual cold work and fine grain size were responsible for the join strength.

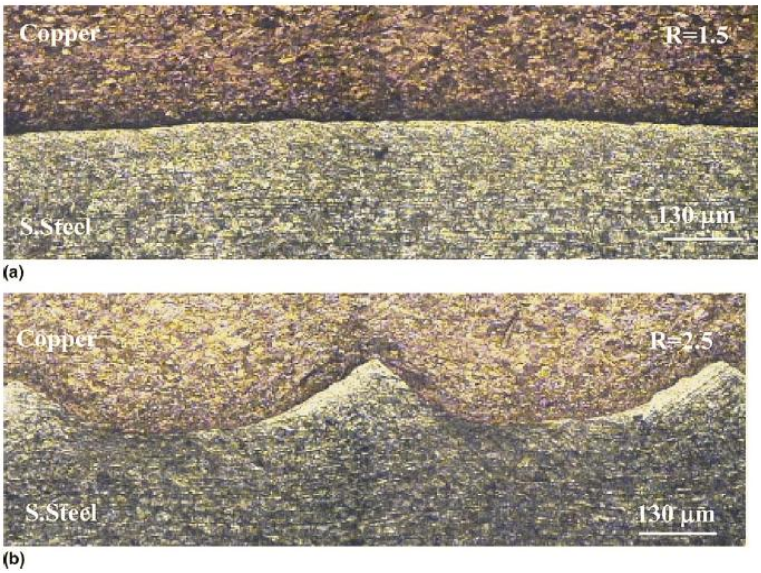

Figure 2.1 - Interface view of join with a straight (a) and wavy morphologies (b) [21].

2.3.4. **Diffusion bonding**

Diffusion bonding is another process being the key parameters: temperature, pressure, time and surface roughness of the materials [2, 4, 23, 24]. The bonding is made along the interface, so it is an advisable technique for joining similar or dissimilar metals, particularly involving large areas [25] but it has the disadvantage of forming a thick layer of intermetallic compounds at the interface, decreasing the joint strength. Moreover, it needs complex equipment (e.g. a vacuum chamber with protective gas, heating coils, etc) [25].

Yilmaz and Çelik [8] showed that, through metallographic studies of diffusion bonding of electrolytic Cu and 304 stainless steel, there was good bonding at temperatures of 800 to 850 ºC, pressures of 4 to 6.5 MPa and bonding times of 15 - 20 min. These authors investigated the electrical conductivity of samples between 260 - 370 K and concluded that defects increased the electrical resistivity. However, the intermetallic layer formed at the interface did not have an electrical resistivity sufficiently high to vary the resistivity of the joint. It was also reported that the bimetallic thermal conductivity varied with the change of direction in the electric current, due to the different phases of the intermetallic interface, with distinct values of thermal conductivity. Yilmaz and Aksoy [26] accounted Kirkendall effect: different diffusion coefficients of the materials, was the cause of micro-voids and micro-cracks that damage the mechanical and physical properties of the joint. The best quality joints in Copper to 304 stainless steel were obtained at temperatures of 800 - 850 ºC at 10 MPa, which was pressure the most important parameter for reduced Kirkendall effect.

Some authors applied a compatible interlayer on the interface, due to the high difference in thermal coefficients of both metals, where typically all the elements being joined are present due to interdiffusion. Xiong et al. [11] conducted the joining of stainless steel to copper through the diffusion bonding with the help of interlayer metals. Interlayers of tin-bronze (TB) were used, as well as, Au, and TB - Au. The fracture occurred in copper base material with a tensile strength of 228 MPa. Increasing the temperature, increases the joint strength since the steel grain boundary near interface is more wetted, increasing the bonding area. The authors stated that if the temperature was low, this effect was small. However if the temperature was high, the strength of copper base metal was weaker, due to the grain growth. Nishi et al. [27] had already proven that it was possible to bond alumina dispersion-strengthened copper (DS Cu) to 316 stainless steel with interlayer metals (Au, Cu and Ni foil). The objective was to prevent the formation of brittle intermetallic compounds. The strongest joints were performed under a bonding temperature of 850 ºC, under a pressure of 4.8 to 9.8 MPa. With the same pressure and holding time of 1 hour, that fractured on the DS Cu base material. Sabetghadam et al. [10] showed the join of copper to 410 martensitic stainless steel with a nickel interlayer. The best results in shear strength (145 MPa) were obtained when joining at 900 ºC temperature, under 12 MPa and 1 hour of applied pressure. Nevertheless, these results presented Kirkendall voids that increased with higher joining temperatures and causing a lower strength of joint, confirming previous researches

[26, 28]. Another study reports that it is possible to join Cu-Cr-Zr alloy to 316 stainless steel without porosity or cracks by a nickel interlayer [29].

2.3.5. **Friction Stir Diffusion Process**

Friction stir diffusion process (FSDP) is a new technology based on friction stir welding (FSW), which was developed and patented by The Welding Institute (TWI) in 1991. Initially applied to aluminum alloys to prevent defects common of fusion welding, is a process with a potential to join dissimilar materials. Recently, interesting studies came up on welding dissimilar materials [1, 30].

FSW uses a non-consumable rotating tool, constituted by probe and shoulder, that plunges into plates to be joined until the shoulder contacts with the material (Figure 2.2). The heat generated by friction raises the material temperature and its ductility and viscoplasticity facilitating material flow while the tool travels along the joint [30, 31]. This process is seen a environmentally friendly due to low levels of noise, energy efficiency (about 2.5 % of the energy required for laser welding) [32], and shielding gas is not necessary.

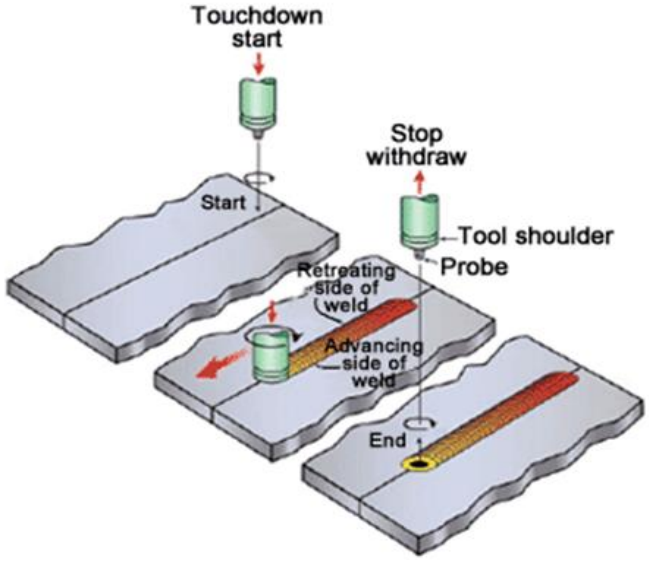

Figure 2.2 - Schematic representation of FSW process [33].

The main parameters of FSW are rotating speed, traverse speed, axial forging force and tool geometry (Figure 2.3). However, these are constrained by material characteristics such as the melting point and physical properties of the material, which is undesirable to achieve [30].

FSW is a process that produces asymmetric welds. The side of the weld where the tool rotation direction is the same as the traverse direction, is referred as the advancing side (AS), while the retreating side (RS), in which the directions of tool rotation and traverse direction are opposite [1, 12, 34], as shown in Figure 2.3.

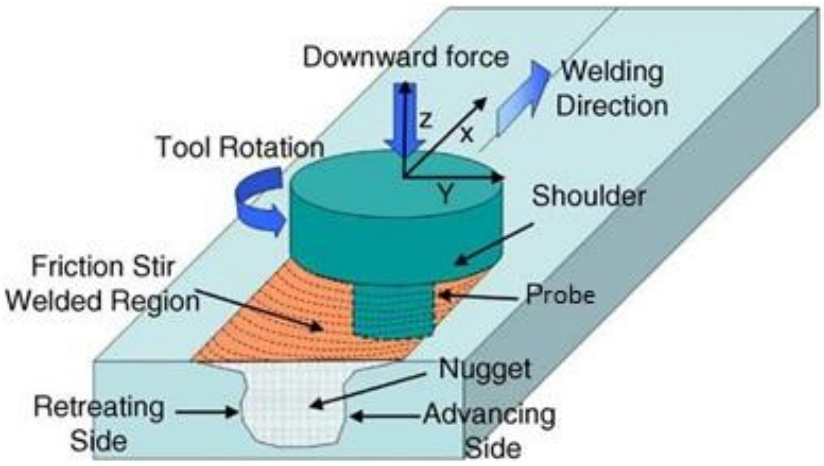

Figure 2.3 - Schematic diagram of FSW [30].

The weld is divided into three or four regions, as shown in Figure 2.4. Zone A is the base material which is not deformed or affected by the process. The zone B is known as the heat affected zone (HAZ) but no plastic deformation occurs. Zone C is affected by the deformation and heat and is given the name of thermo-mechanically affected zone (TMAZ). In case of some materials, a nugget is formed, which is a dynamically recrystallised zone (Zone D) [12, 34].

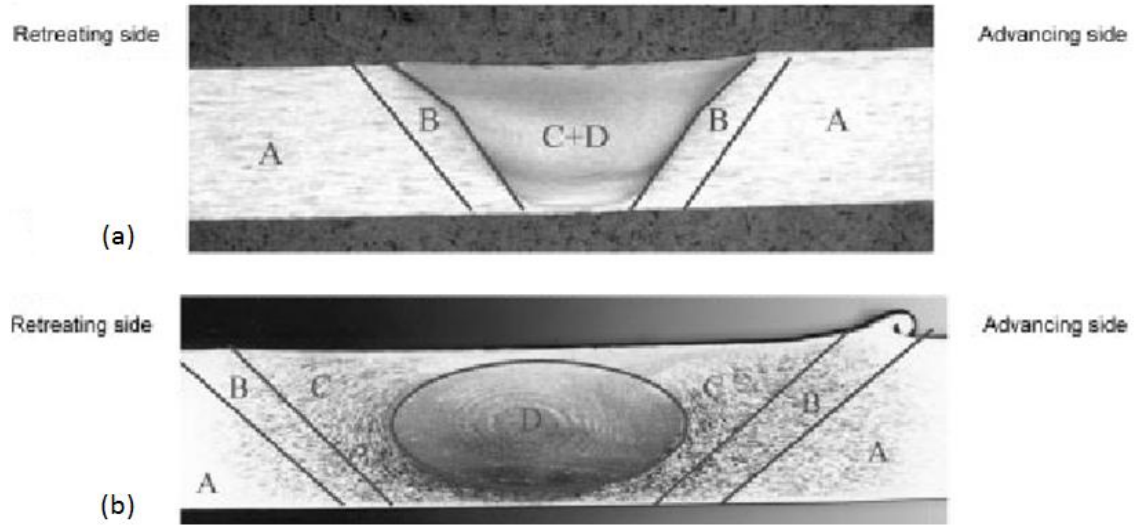

Figure 2.4 - Macrosections of FSW (a) in aluminium alloy with distinct nugget region, (b) in titanium alloy without distinct nugget region [34].

Tool wear can be disregarded for low melting point materials (Al, Mg and Cu alloys) while for joining materials with high melting point (steel and titanium), it is a critical issue. There are some materials that support temperatures above 1000 ºC (tungsten carbide, W alloys and Mo alloys), but are very difficult to machine [30, 35]. The selection of the tool's material is an important factor, due to tool wear, that influences the microstructure, heat generation and dissipation, weld quality and the processing cost [36]. The tool shape needs to be as simple as

possible, to reduce the cost and sufficient stirring effect to produce good sound welds [35]. The non-consumable rotating tool is constituted by a shoulder and probe that it can be of different sizes and shapes, and which are responsible for heat generation and material flow [36]. The probe or pin, can be cylindrical, conical or convex, flat faced, threaded or fluted.

Although the effect of tool shape has not yet been sufficiently studied, Colegrove et al. [37-41] demonstrated that the profiled probe designs (Triflute) to model of aluminium alloys, had small effect on the heat generated, contrary to what the change in the shoulder contact radius can cause. Trivex tool has good ability to stir the material and minimize the downwards forces, having higher or equal benefits to MX Triflute TM tool.

There are several different types of shoulder designs: flat, convex, concave, featuring grooves, ridges, scrolls or concentric circles [42].

FSDP promotes joining only by the diffusion of heat generated between the tool and one of the metals (preferably those with the lowest melting point), unlike the FSW that joints both metals by diffusion and plastic strain, as shown in Figure 2.7. This is the main difference between these two processes.

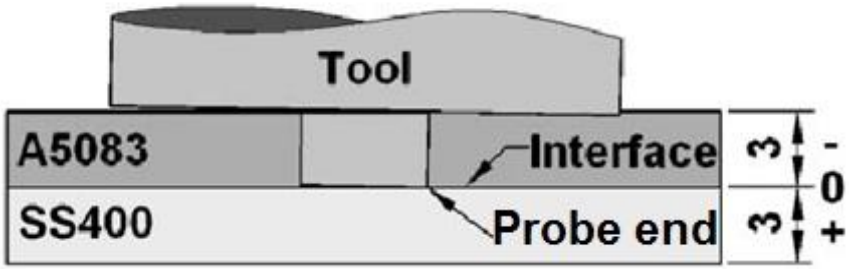

Figure 2.7 - Example of FSDP to lap joint configuration with zero offset of probe depth [43].

There are few studies on the FSDP and none reports on copper-steel joints. The following researchers have studied lap joints through the FSW but with similar parameters to those of FSDP.

Elrefaey et al [44] successfully joined A1100H24 aluminium alloy to a low carbon steel. It was observed that when the probe depth was inside the steel (offset + 0.1 mm), the lap joint has a meaning effect on the shear load, compared to a probe offset of 0 (probe depth in aluminium) and the joint showed very low strength. The hardness values in the base steel were of 116 HV but after weld, the fine grain steel zone was harder (170 HV). On the aluminium it remained almost constant, around 30 HV. At the interface of the joint a higher value of hardness was observed due to the formation of an IMC in the hard structure (the average hardness around 300 HV) and brittle. The two joints that had higher strength were also the only ones that did not fractured at the weld line. That occurred mainly in the aluminium (in the layered structure) due to IMC presence.

K. Kimapong and T. Watanabe [43, 45] could do lap joint of A5083 aluminum alloy and steel SS400. The authors refer that the heat conduction is negligible, so the reason for the increase in IMC phase with peak temperature was wit unclear. This study attempted to understand the effect of rotational speed, traverse speed, probe depth, tool tilt angle, diameter of probe and pre-hole diameter. As shown in Figures 2.8 and 2.9, increasing the traverse speed and pre-hole diameter there was a decrease of heat generated and hence lower IMC thickness. Moreover, IMC thickness increases with increasing rotational speed, probe depth, tool tilt angle or probe diameter. At the end of each study, the parameter which has been chosen around at higher shear loads and minimal IMC thickness. After this study, the maximum force recorded was of 130 MPa, about 77% of strength of the aluminum base material and no IMC was observed. The parameters used were a rotating speed of 225 rpm, traverse speed of 0,73 mm/s, a probe depth 0,1 mm on the substrate, 1 º tool tilt angle, 5 mm probe diameter and 10 mm pre-hole diameter. The tool material was JIS-SKH57 steel and a shoulder diameter of 20 mm were fixed.

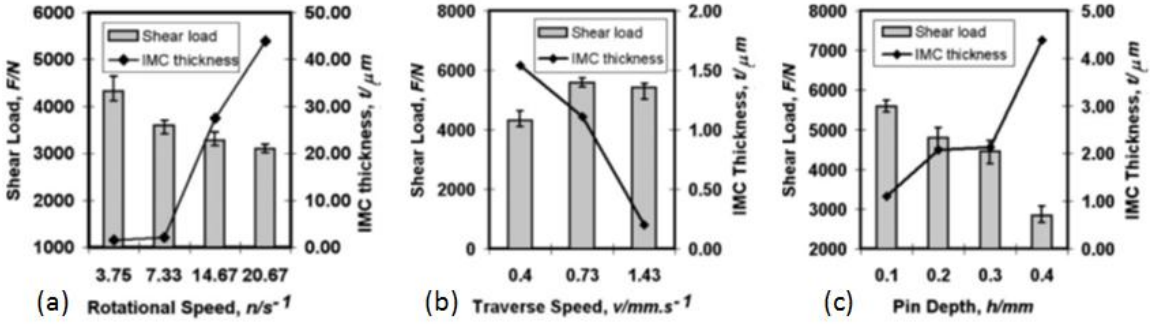

Figure 2.8 - Relationship of the parameters with shear load and IMC thickness; (a) rotational speed. (b) Traverse speed. (c) Probe Depth [43].

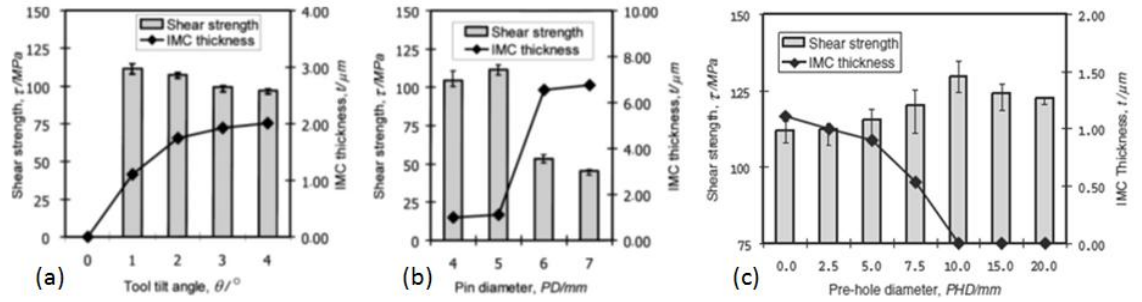

Figure 2.9 - Relationship of the parameters with shear load and IMC thickness; (a) Tool tilt angles. (b) Probe diameter. (c) Pre-hole diameter [45].

Abdollah-Zadeh et al [46] in the lap joints of aluminum with copper, have reported joints stronger than the aluminum base material. Vahid Firouzdor and Sindo Kou [47] had an idea of a modified lap (Figure 2.10) which increases nearly twice the joint strength and ductility between five to nine times, compared to conventional lap joints. However, in both articles [46, 47], the probe needed to penetrate the substrate (copper) by 0.1 to 0.2 mm, to generate more heat near the interface.

Figure 2.10 - Conventional and modified lap joint [47].

Multi-pass technique has not been fully described, however the work on aluminium could give some insights into the multiple-pass technique on copper joints. Gandra [33] proposed the overlapping on the advancing side, once the hardness is higher than that in the overlapping on the retreating side. Furthermore, Nascimento [48] defined an equation of overlapping ratio (OR):

$$OR = 1 - \left[\frac{l}{d_{probe}}\right] \tag{2.1}$$

Where: l represents the distance between probe centers in two successive passes and d_{probe} is the probe diameter. According with this [48], the use of a cylindrical probe requires a minimum value of OR = 0.5, in order to obtain a uniform hardness distribution, through the nuggets interpenetration which leaded to a homogeneous processed area.

Table 2.1 - Summary table showing the characteristics of the joining or cladding processes.

	Laser cladding	HIP	Explosive cladding	Difusion bonding	FSDP
Time	low	high	low	high	low
Area	small	high	high	high	small
Energy comsumption	low	moderate	high energy explosion	moderate	very low
Environmental aspects	inert gas stream, light emissions, consumable materials	vacuum chamber with inert gas shielding, interlayer, polishing or machining and clean	high levels of noise, vibration, vacuum chambers, clean surface	vacuum chamber or inert gas shielding, interlayer, resistance heating, polishing or machining and clean	polishing and clean

Metallurgical	discontinuities, lack of homogeneity, intermetallic	need heat treatment, intermetallic	higher shear and tensile strengths, fine microstructure, may require heat treatment	Intermetallic, grain growth	excellent properties at the joint area, fine microstructure
Technical aspects	single pass, high welding speeds, automated process	automated process, multi step technique	manual process, limited flexibility	automated process	one-step technique, automated process, can operate in all positions

2.4. Conclusion

FSDP is a recently developed variant of FSW that can joint different materials through a locally rapid diffusion process in a simple automated process for joining or cladding small parts.

Since it is a solid state joining process, the thickness of intermetallic compounds at the interface of the joint can be minimized, improving the overall mechanical strength of the joints.

The heat is generated from friction and plastic deformation so it has low energy consumption (only 2.5 % of the energy required for laser weld).

It is a environmentally friendly joining, clean and not pollutant since it has no fumes, light emissions, consumable materials, shielding gas, high levels of noise or vibration.

3. Experimental set-up

3.1. Materials characterization

In this study, the following materials were used: a commercially pure copper with 1.1 mm thick, provided by SIEMENS.

304 stainless steel with two different thicknesses: 1 and 6 mm. This material was supplied by IMS, who also provided chemical and mechanical properties information, as presented in Table 3.1 and 3.2.

Table 3.1 - 304 stainless steel chemical composition.

Chemical composition (weight %)								
	C	Cr	Mn	N	Ni	P	S	Si
1 mm x 1250 mm x 2500 mm	0,025	18,155	1,789	0,072	8,011	0,033	0,003	0,239
6 mm x 150 mm x 6000 mm	0,022	18,041	1,269	0,0333	8,068	0,0209	0,0058	0,391

Table 3.2 - 304 stainless steel mechanical properties.

Mechanical properties				
	Rm (N/mm^2)	Rp 0,2 (N/mm^2)	Rp 1,0 (N/mm^2)	A %
1 mm x 1250 mm x 2500 mm	623,21	306,2	342	55,74
6 mm x 150 mm x 6000 mm	603	469	496	52,8

3.2. Equipment

3.2.1. **Machine**

To produce lap joints by FSDP it used an ESAB LEGIO™ 3UL numerically controlled machine, with three degrees of freedom.

The process parameters can be adjusted before or during operation, being recorded in a data acquisition system (SCADA). The machine parameters were:

- Rotation speed (rev/min)
- Travel speed (cm/min)
- Downward force (Kg)
- Tool position in X, Y, Z (mm)

- Plunge speed (mm/s)
- Dwell time (s)
- Control method (force or position control)

The machine comprises a structure and table fixed, which allow some working positions, depending on the guide of the table and the fastening system. As shown in Figure 3.1, the machine is further constituted by an human machine interface (HMI) dashboard controlling the process parameters (except tilt angle), a welding head with freedom of movement in X, Y, Z, the power unit and an internal water cooling system to cool the spindle shaft and the tool. The tilt angle (0° to 5°) can be adjusted manually by rotation of the welding head relatively to the axis Y. The direction of tool rotation is clockwise. The hydraulic cylinder that controls the force applied to the Z axis and the forging tool movement, can be used in position or load control. By choosing the position control, the machine will hold position during the process, causing adjusting the load. However, if the preference is the force control, the machine will maintain the force throughout the process, adjusting the tool position, thereby making the process more constant throughout the welding, since the worktable may have small slopes.

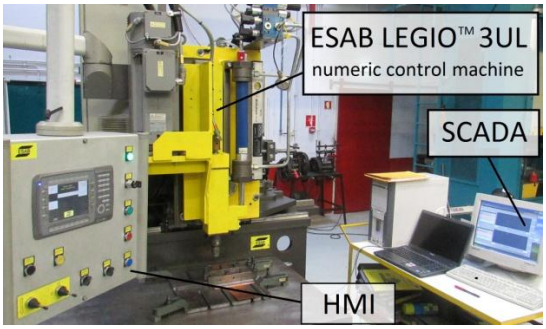

Figure 3.1 – ESAB LEGIO™ 3UL numeric control machine.

3.2.2. **Tool Design**

The geometry of the tool is essential for the development of this technology, since it controls the material flow, the heat dissipation and must withstand mechanical stress. In this work, it was used an adjustable modular tool called iSTIRtool_v3 (Figure 3.2), developed and patented by Santos and Vilaça [49] at IST-UTL. The tool body which is the structural component, allows the entry of different combinations of geometric parameters of probe and shoulder, fastened by screws. The probe can be readily adjusted to the desired height for the processing of different thicknesses. This tool is suitable for cooling channel from the machine, cooling all components of the tool. The height of the probe can be adjustable at any time by screwing or unscrewing the shoulder in the tool body. This adjustment has 12 positions at every step of 1 mm high.

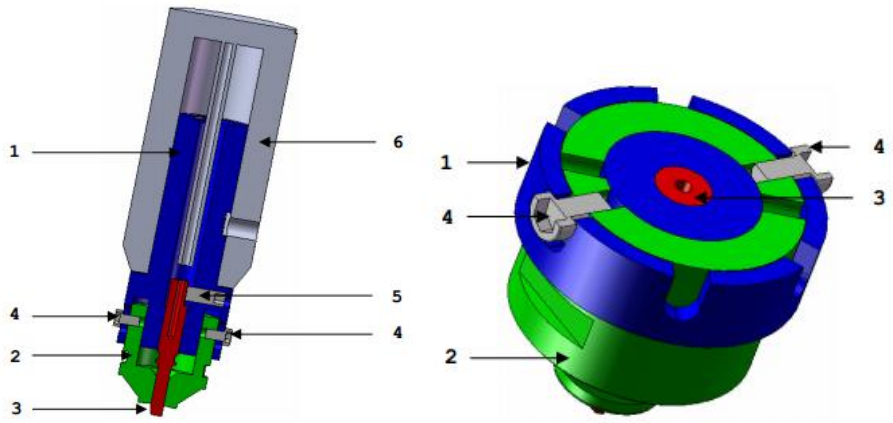

Figure 3.2 - iSTIRtool_v3 tool. (a) Longitudinal section view, (b) Cross section view. 1 - Tool body; 2 - Probe; 3 - Shoulder; 4 - Shoulder fixation screw; 5 - Probe fixation screw; 6 - Machine spindle shaft [49].

As this work intends to study the binding of overlapping plates, and since the rotation is clockwise, it was used a left-hand threaded cylindrical probe to have a three-dimensional downwards flow, forging the materials against the backplate [50]. The shoulder chosen is constituted by two grooves which describe one full turn while providing good control flow on the material surface (Figure 3.3). The probe with 5 mm diameter and the shoulder with 16 mm diameter are made of AISI H13 steel while the body of the tool was built from DIN Ck45 steel.

Figure 3.3 - Threaded cylindrical probe and shoulder groove with two one-lap ridge.

3.2.3. **Fixturing system**

The fixing is an important requirement to produce good processing qualities. Its function is to press the plates against one another so as to be fixed and flat, being in contact throughout its length. The forces applied by the machine and the friction generated between the tool and the material, increase the temperature and plates deformation so they need to be rigidly clamped. This system allows the use of plates 200 mm wide and 350 mm long.

The fixturing system consists of two bars which, together with screws, apply the clamping force. The larger screws clamp in the base plate whilst the lower screw press the plates that unify the clamping force on the plates to process.

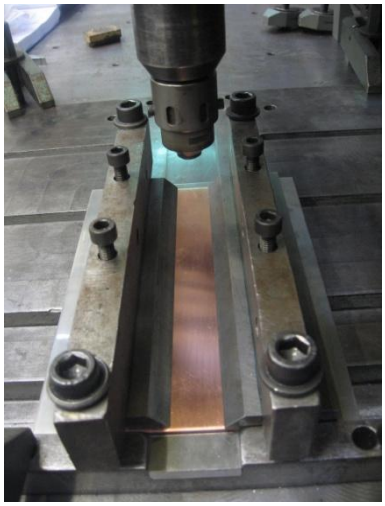

Figure 3.4 – Fixturing system.

3.3. Working methodology

3.3.1. **Plates preparation**

From the original materials, the dimensions of the plates were chosen appropriate to the fastening system available minimizing material wastes and maximizing the number of welds per plate. In case of stainless steel plates, it was important to keep the width and length, for both thicknesses, to study the effect of thermal diffusion. Contrary to stainless steel, this effect does not occur in copper as it has high thermal conductivity and the heat generated is transferred to the tool and the substrate. Considering these aspects, size of the plates were as follows (Figure 3.5): Type 1) copper plate: 1.1 mm x 100 mm x 200 mm; stainless steel plate: 1 mm x 150 mm x 200 mm. Type 2) copper plate: 1.1 mm x 150 mm x 200 mm; stainless steel plate: 6 mm x 150 mm x 200 mm. Copper and SS plates were cut with a guillotine and SS bars with a saw ribbon to produce samples for FSDP.

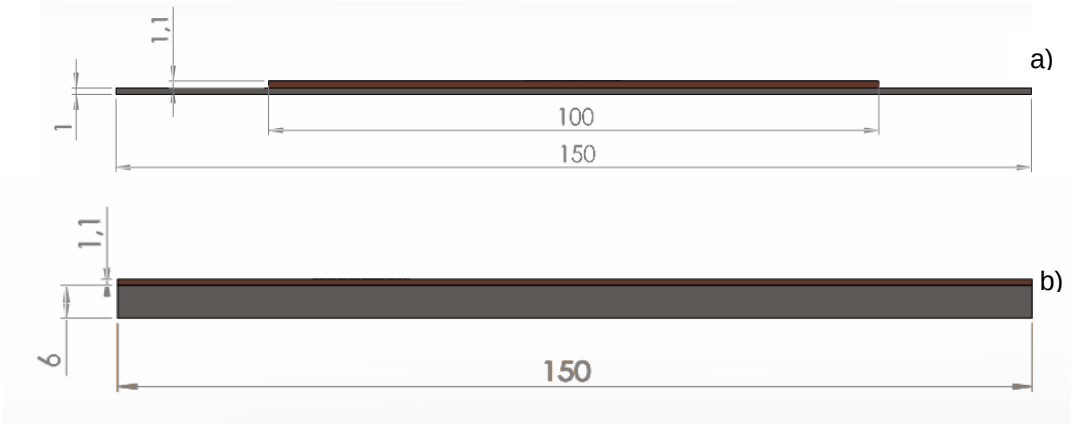

Figure 3.5 – Cross view of the joint. (a) Type 1, (b) Type 2.

Surfaces cleaning was by sanding plates in order to remove the oxide layer. For this, it used sandpaper 240 and 600. Then, compressed air was used to withdraw the dust due to the sanding. Finally, the surfaces were cleaned with alcohol or acetone.

3.3.2. **Selection of parameters**

The criterion optimization for experimental parameters presented by K. Kimapong and T. Watanabe [43, 45] is valid but may not be effective to find the parameters that correspond to the maximum strength supported by the joint. Abdollah-Zadeh et al [46] made an array with two important parameters: rotation speed and travel speed, to understand their effects on the joint strength and find the set of parameters leading to higher mechanical strength. In this case the best results were obtained for ratios between 15.8 and 7.9.

Due to a insufficient published data, a matrix of processing parameters was built in order to assess the effects of rotation and travel speeds on the joint characteristics evaluated by joined length in a first approach. Tables 3.3 and 3.4 show the parameters chosen. The parameters used at the beginning of the plate are identified as processed in Stationary Zone (SZ), while the parameters used at the end of the plate are identified as processed Near to Edge Zone (NtEZ), as shown in Figure 3.6. Joints type 1 (using 1 mm thick stainless steel) and type 2 (using 6 mm thick stainless steel) have some common parameters in order to compare the binding to different thicknesses. However, the type 2 joint were used parameters that provide more heat, due to having more material to heat. All other parameters were fixed, as shown the Table 3.5. The probe had to be as near as possible but without touching the substrate, to avoid tool damage. Four trials were made by connecting copper (thickness = 1.1 mm) to carbon steel (thickness = 1.2 mm) with loads between 7000 to 5500 N in order to assess possible parameters. Sample with 5500 N produced the greatest joining widths. The tool tilt angle was chosen to be zero in order to avoid the restrictions at the welding direction.

Table 3.3 - Rotation and travel speeds used in FSDP of lap joint type 1 with respective indication of $\Omega / \vartheta x$ ratio, sample reference and joining zone.

	Rotation speed (rev/min)				
	800	1000	1200	1400	1600
Travel speed (mm/min)					
60	13.3 (H20, SZ)	16.7 (H5, NtEZ)	20 (H12, SZ)	23.3 (H16, SZ)	-
90	8.9 (H17, NtEZ)	11.1 (H4, SZ)	13.3 (H8, SZ)	15.6 (H14, SZ)	-
120	6.7 (H19, NtEZ)	8.3 (H6, SZ)	10 (H10, SZ)	11.7 (H18, SZ)	13.3 (H22, SZ)
150	-	6.7 (H7, NtEZ)	8 (H11, NtEZ)	9.3 (H13, NtEZ)	10.7 (H21, NtEZ)
180	-	-	6.7 (H9, NtEZ)	7.8 (H15, NtEZ)	8.9 (H23, NtEZ)

Table 3.4 - Rotation and travel speeds used in FSDP of lap joint type 2 with respective Ω / ϑx ratio and sample reference.

	Rotation speed (rev/min)				
	1200	1400	1600	1800	2000
Travel speed (mm/min)					
60	20 (I12, SZ)	23.3 (I16, SZ)	26.7 (I25, SZ)	-	-
90	13.3 (I8, NtEZ)	15.6 (I14, SZ)	17.8 (I24, SZ)	20 (I30, NtEZ)	-
120	-	11.7 (I18, NtEZ)	13.3 (I22, SZ)	15 (I27, SZ)	-
150	-	9.3 (I13, NtEZ)	10.7 (I21, NtEZ)	12 (I28, NtEZ)	-
180	-	-	-	10 (I26, NtEZ)	11.1 (I29, NtEZ)

Table 3.5 - Fixed FSDP parameters.

Welding position (mm)	**Probe length (mm)**	**Plunge speed (mm/s)**	**Dwell time (s)**	**Downward force (N)**	**Tool tilt angle (º)**
- 1	0.92	- 0.1	5	5500	0

As the joints type 2 have a thickness exceeding 3 times the thin joints, load tests were performed varying the downward force of 500 N up and below, of the previously set value. Table 3.6 shows the sample reference for different downward force for fixed parameters of 1600 rev.min^{-1} and 120 mm.min^{-1} to rotation and travel speeds, respectively.

Table 3.6 - Downward force used in FSDP of lap joint type 2 with fixed parameters of rotation and travel speeds with sample reference.

	Downward force (N)		
	5000	5500	6000
Ω | ϑ_x (rev.min^{-1} | mm.min^{-1})			
1600 | 120	I 22 C (NtEZ)	I 22 (SZ)	I 22 B (NtEZ)

To produce consistent results, the samples were cut in the same section after the process stabilized. The samples produced with the parameters marked in Stationary Zone were cut at 20 mm from the end, whereas those produced with parameters marked in Near to Edge Zone were cut to 30 mm to avoid significant variations in joined width to face positioning of the joint, due to the edge effect .

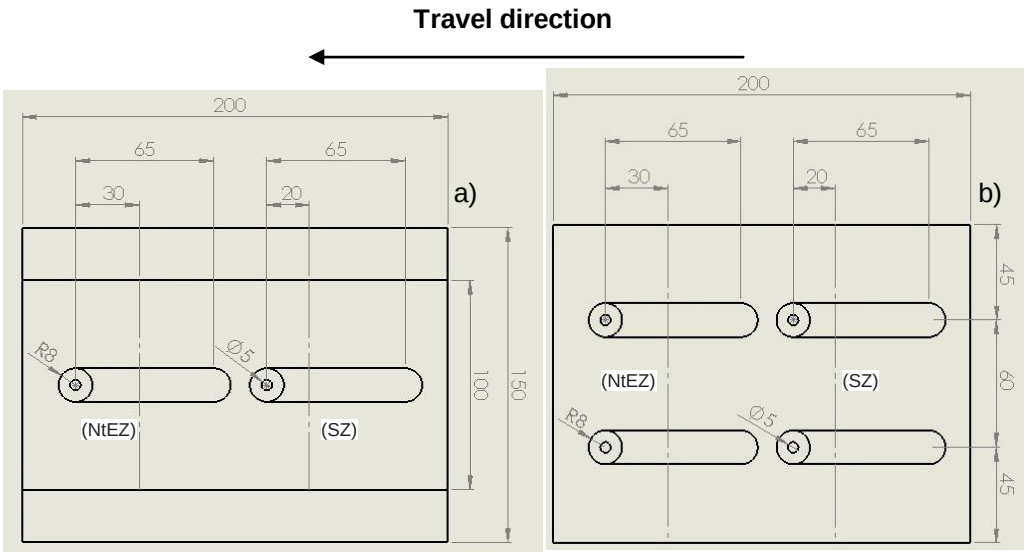

Figure 3.6 – Drawing of the FSDP joints for metallography (dimensions in mm) (a) type 1 and (b) type 2.

Multi-pass were performed by overlapping on the advancing side with an OR = 0.5 ratio, ensuring a uniform hardness and microstructural characterization stable [32, 48].

3.4. Characterization techniques

3.4.1. **Metallography**

To perform metallographic analysis, samples were polished to identify existing defects and measure the joined width on the interface. Thereafter, some samples were selected to be etched and to evaluate the microstructural transformations in each material. The preparation of metallographic samples is described in annex A.

An inverted optical microscope Leica DMI 5000 M was used.

3.4.2. **SEM/EDS**

For a deeper evaluation of the interface, it was used a scanning electron microscopy (SEM) equipped with energy dispersive spectroscopy (EDS). These observations were performed with secondary (SE) and back-scattered electrons (BSE).

3.4.3. **Hardness Testing**

Hardness tests were conducted on cross sections of processed joints, parallel and transverse direction to the interface. The machine used was a Mitutoyo HM-112 Micro-Vickers Hardness Testing Machine.

Transverse indentations in the centre of the processing were performed. In the copper plate the tests had a distance of 0.2 mm from the surface and to each other, while in stainless

steel the distance was of 0.12 mm, due to the a greater hardness than that of copper and the objective to see the effects on hardness due to concentration of heat, in the area near the interface. The hardness profile parallel to the interface, which was performed only on copper, had a distance from the processed surface of 0.2 mm and 0.4 mm between indentations. The load used in the micro hardness tests was 200 g and the dwell time of 10 s.

3.4.4. **Shear Tests**

Tensile tests were performed using an AUTOGRAPH SHIMADZU model AG500Kng equipped with a load cell capacity of 50 kN, and test speed of 3 mm/min. In order to avoid application of moments on the joints, plates were placed in the clamping system to compensate variations in thickness (Figure 3.7).

Figure 3.7 - Shear test set-up.

Three specimens were tested for each joining condition having general dimensions shown in Figure 3.8, except for sample I 22 4S OR = 0.5 (Figure 3.9). These samples were milled edges with a 240 grinding paper to reduce stress concentration points. Shear tests were performed according to the steps shown procedure presented in annex C.

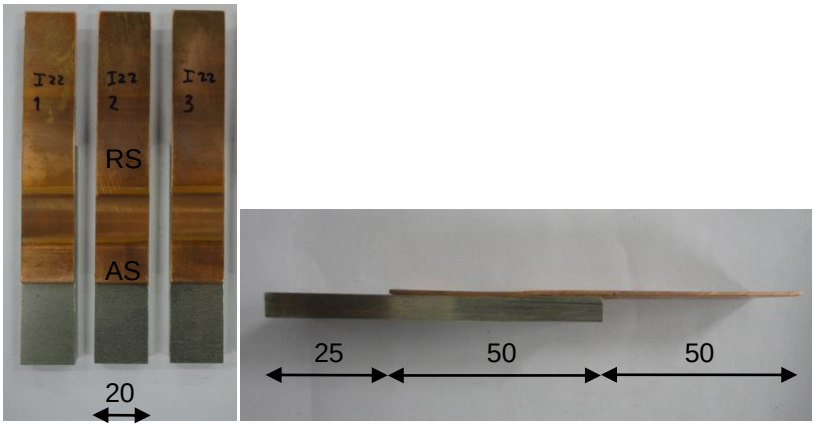

Figure 3.8 - Test specimens I 22 (dimensions in mm).

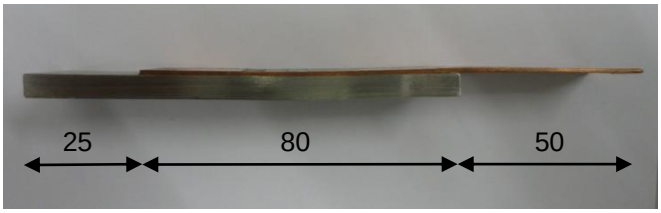

Figure 3.9 - Test specimen I 22 4S OR = 0.5 (dimensions in mm).

3.4.5. **Bending Tests**

Three-point bending tests followed EN 910 (1996) [51] for choosing the diameter of the former and distance between rollers. The diameter was set at 16 mm and the distance between rollers was 22 mm for joints type 1 and 37 mm for joints type 2. The tests were performed in the transverse direction to the face processed, as shown in Figure 3.10.

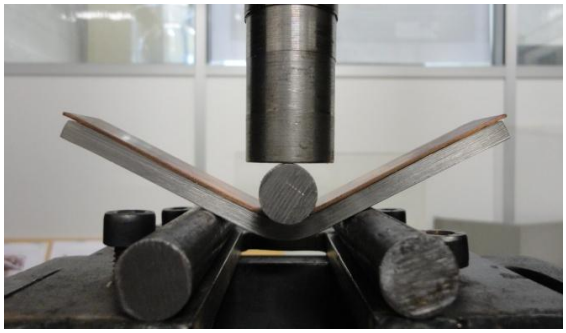

Figure 3.10 - Bending test.

For bending tests the same machine and grinding process were used with a downward speed was 5 mm/min. The overall dimensions of the specimens are shown in Figure 3.11 with three specimens per joining conditions, except I 22 4S OR = 0.5 only two specimens were tested. Bending tests were performed according to the procedure presented in annex C.

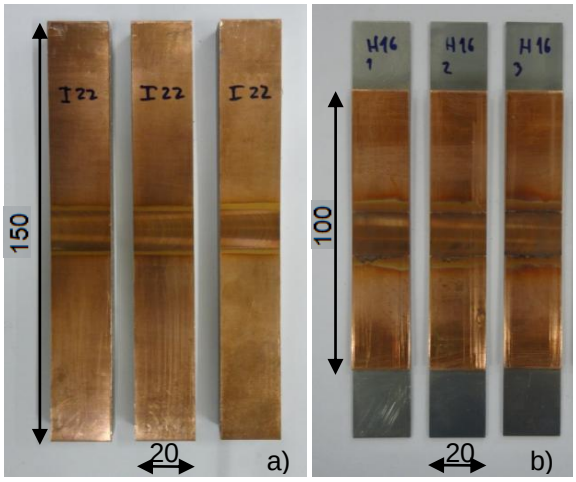

Figure 3.11 - Test specimens. (a) Type 2 joints and (b) Type 1 joints (dimensions in mm).

3.5. Conclusion

In this chapter a description was presented on the materials and methods adopted in this research.

As far as experimental methods are concerned, a description of methodology for FSDP and characterization test was provided.

4. Results and discussion

4.1. Base material

Base material was characterized in order to observe its microstructure and hardness. Samples were cut, polished and etched in the section parallel to the surface.

Micrograph of pure copper is presented in Figure 4.1. The material showed an anisotropic structure of elongated grain, due to cold rolling and partially annealed operations.

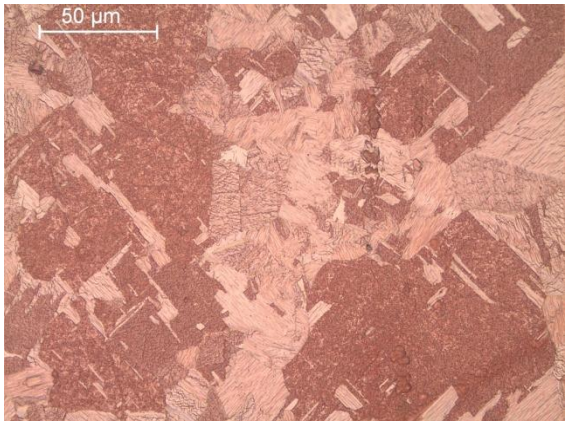

Figure 4.1 – Micrograph of copper plate.

Micrographs of 304 stainless steel (Figure 4.2), for 1 and 6 mm of thickness, showed a structure of elongated grain, originated by cold working and annealing operations.

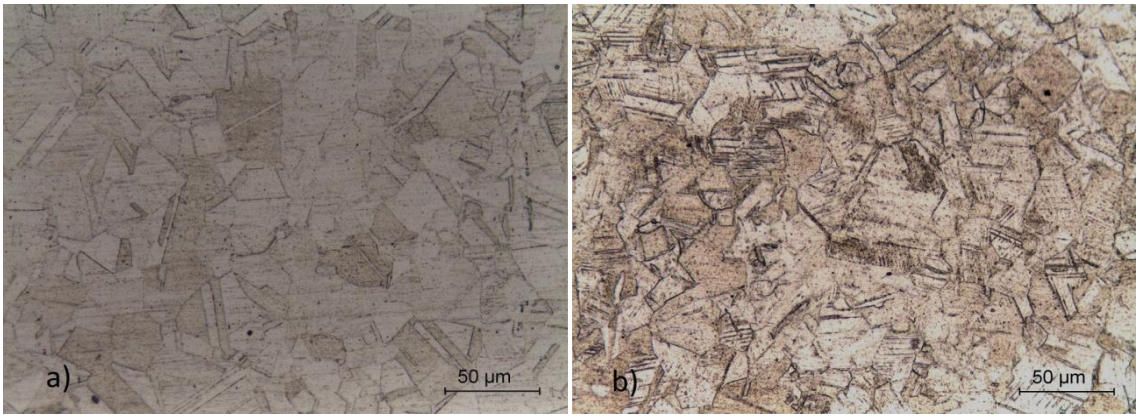

Figure 4.2 – Micrographs of stainless steel plates. (a) Thickness of 1 mm; (b) Thickness of 6 mm.

Six micro-indentations were performed under a load of 200 g, calculating its mean and standard deviation presented in Table 4.1. Through these hardness measurements it is understood that heat treatment contributed to improve the homogeneity of the material.

Table 4.1 – Hardness measurements of base materials.

HV 0.2	Cu	SS (1 mm)	SS (6 mm)
Average	65.07	184.58	236.18
Standard deviation	± 0.37	± 3.13	± 6.38

Figure 4.3 shows the true stress-true strain curve of copper with maximums values of 255.3 MPa and 0.350.

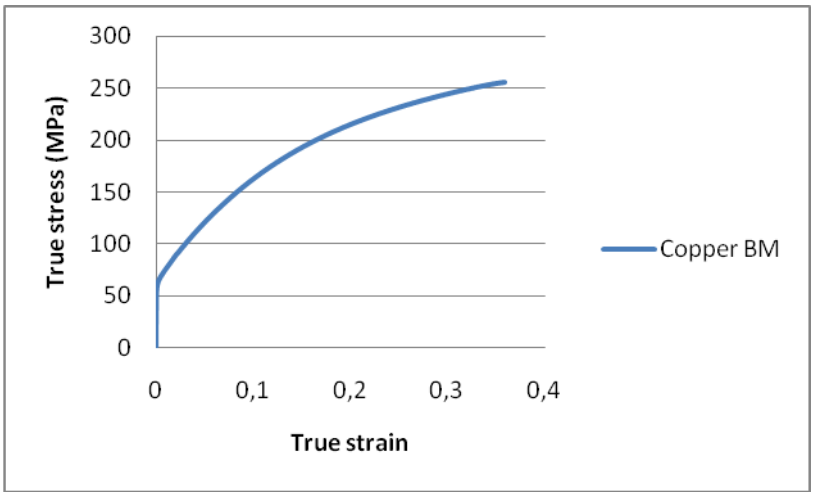

Figure 4.3 - Tensile test true stress-true strain curves of copper base material.

4.2. Metallurgical characterization of joints

This subchapter aims to assess the changes made by FSDP due to heat generated by friction between the tool and the copper plate and applied pressure are responsible for these changes. Thus, it is intended to identify the effect of the parameters on the surface, the bonded width of the joint and geometric details caused by processing, microstructural changes and SEM/EDS analysis at the interface of materials.

4.2.1. **Visual analysis**

To analyze the visual characteristics of the joints, macrographs taken for all samples. Table 4.2 presents the effects found when different parameters of rotation and travel speeds used in type 1 samples. H 20 and H 7 samples showed color gradients in processing. It was observed that for rotation speeds of 800 rev/min bonding was never achieved independently of the travel speeds tested. In sample H 5 a defect was observed leading to excessive penetration of the tool. This may be linked to two factors: the proximity of the plate edge which causes a temperature rise in the material or due to the waves of the copper plate, as in sample H 16, since this is a high ductility material. Visually, the sample H 5 failed to stabilize, therefore it was removed from subsequent analysis. Samples H 22 and H 16 exhibited a uniform color from the beginning to the

end of processing and with larger areas affected by heat compared to previous samples. H 20 and H 16 samples presented burr in AS, whereas H 7 in the RS. H 22 showed no burr.

Table 4.2 - Top view of the processed samples (type 1) with different parameters of rotation and travel speeds.

Sample	Parameters	Top view
H 20	Ω = 800 rev/min ϑx = 60 mm/min $\Omega / \vartheta x = 13.3$	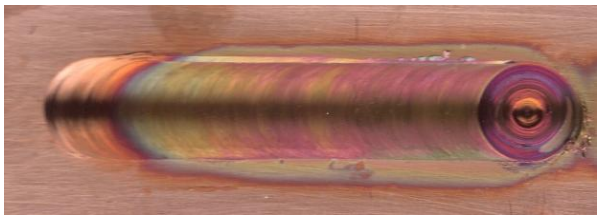 AS RS
H 7	Ω = 1000 rev/min ϑx = 150 mm/min $\Omega / \vartheta x = 6.7$	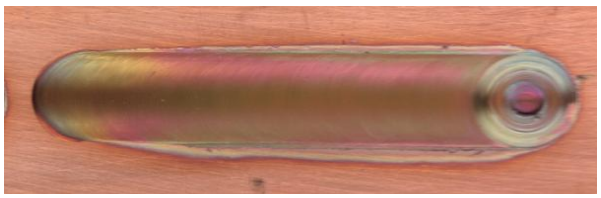 AS RS
H 16	Ω = 1400 rev/min ϑx = 60 mm/min $\Omega / \vartheta x = 23.3$	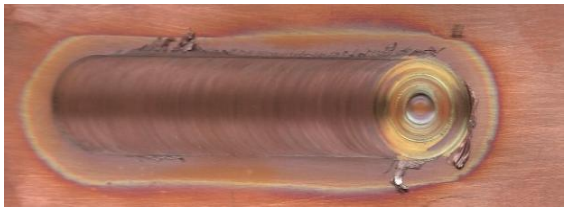 AS RS
H 22	Ω = 1600 rev/min ϑx = 120 mm/min $\Omega / \vartheta x = 13.3$	 AS RS

Joints processing of type 2 are presented in Table 4.3. Apart from variation of the rotation and travel speeds, downward force also changed. The first two samples were processed with the same parameters and tool but different results are obtained. Sample I 16 presents a surface area affected by the heat without burr formation, whereas in sample I 16.2 burr formation existed and tended to increase. This can be caused by equipment and tool instabilities or copper deformation. Sample I 25 had the largest surface area affected by heat. Samples I 25, I 22 and I 26 showed a uniform processed zone free of burrs, such as sample I 16 described above. Sample I 22 B showed a non-uniform mixture of material on the surface and a slight burr on the RS.

Table 4.3 - Top view of the processed samples (type 2) with different parameters of downward force, rotation and travel speeds.

Sample	Parameters	Top view
I 16	Ω = 1400 rev/min ϑx = 60 mm/min Df =5500 N $\Omega / \vartheta x = 23.3$	 AS RS
I 16.2	Ω = 1400 rev/min ϑx = 60 mm/min Df = 5500 N $\Omega / \vartheta x = 23.3$	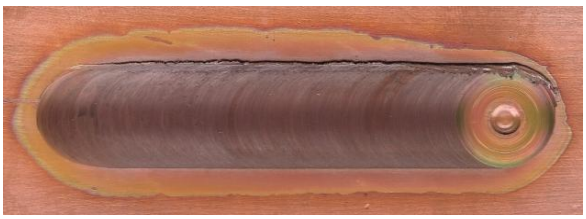 AS RS
I 25	Ω = 1600 rev/min ϑx = 60 mm/min Df = 5500 N $\Omega / \vartheta x = 26.7$	 AS RS
I 22	Ω = 1600 rev/min ϑx = 120 mm/min Df = 5500 N $\Omega / \vartheta x = 13.3$	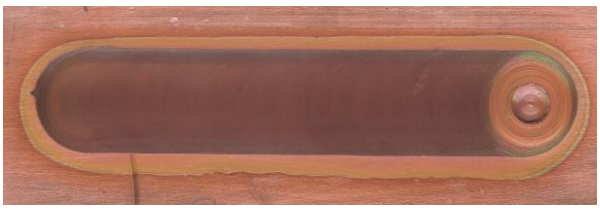 AS RS
I 22 B	Ω = 1600 rev/min ϑx = 120 mm/min Df = 6000 N $\Omega / \vartheta x = 13.3$	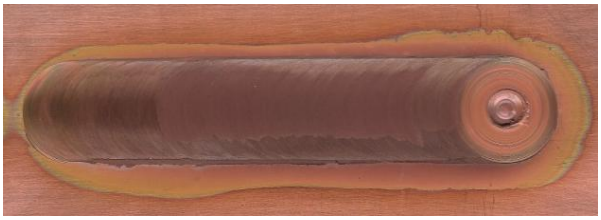 AS RS
I 26	Ω = 1800 rev/min ϑx = 180 mm/min Df = 5500 N $\Omega / \vartheta x = 10$	 AS RS

Multi-pass processing was explored to promote the creation of bimetals with larger widths. Figure 4.4 shows, in general, a good surface of samples I 22 4S OR = 0.5, however, there was a slight burr in the final processing, probably due to unevenness between the processed and unprocessed area. The parameters used were the same as in sample I 22, with 1600 rev/min,

120 mm / min and 5500 N and is composed of four steps overlapping by the AS with an overlapping ratio of 0.5.

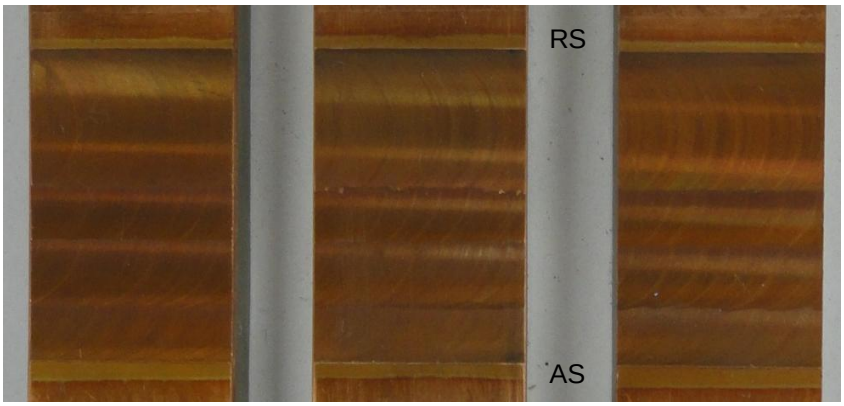

Figure 4.4 - Details of processed surface in sample I 22 4S OR = 0.5 overlapped by the AS.

Despite the use of a solid state processing, three were some distortions, particularly in the thinner plates, due to the fact that there are rapid variations in temperature and the possible lack of heat flow from the stainless steel to the worktable. Figure 4.5 shows the distortion observed in type 1 joint in the center of the plate. This joint was produced with a $\Omega / \vartheta x = 23.3$ ratio, the highest tested, and there was a maximum transverse and longitudinal distortions of 8 mm and 5 mm, respectively.

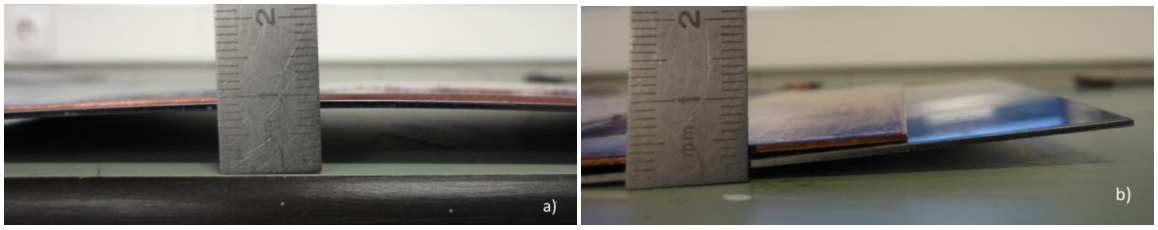

Figure 4.5 - Distortion at the sample H 16 with processing along the plate to bending tests. (a) Side view of the processing, (b) Front view of the processing

Figure 4.6. depicts the deformation observed in type 2 joint with a $\Omega / \vartheta x = 26.7$ ratio and it can be observed that the distortion is substantially smaller due to the higher thickness of stainless steel.

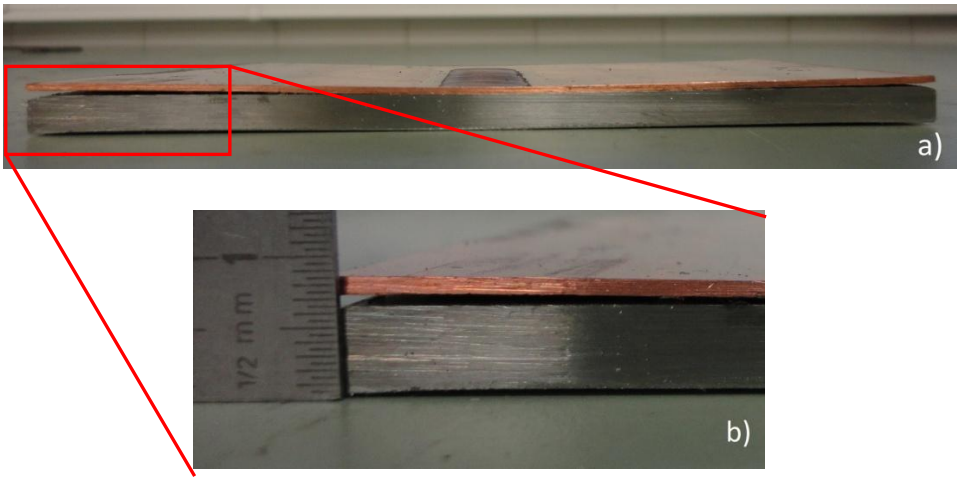

Figure 4.6 - Distortion at the sample I 25 with processing along the plate to bending tests. (a) Cross section view, (b) Detail with distortion measure.

Figure 4.7 shows a cross section view of H 16 sample with a processing along the lateral edge of the plate. In this case the distortion is minimal or nonexistent. The same was found in type 2 joints.

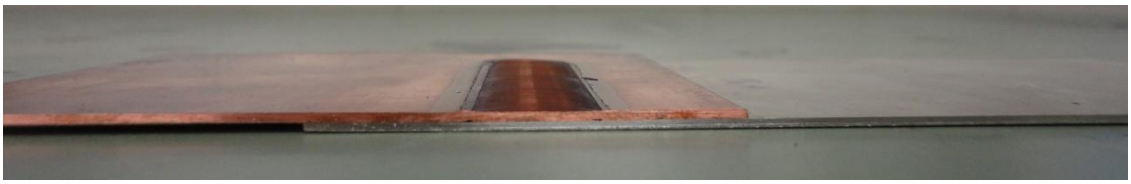

Figure 4.7 - Cross section view of sample H 16 with processing along the plate to shear tests.

A plate processed in four steps is shown in Figure 4.8. The overlapping on the advancing side held the center to the edge of the plate presented a maximum distortion of 1 mm. The parameters used were: 1600 rev/min, 120 mm/min, 5500 N and OR = 0.5.

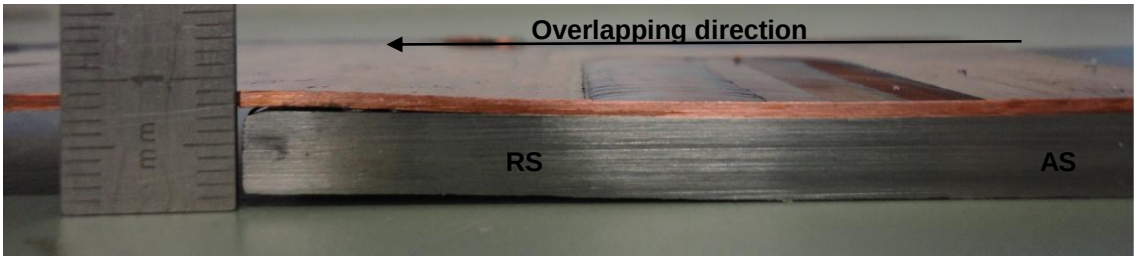

Figure 4.8 - Cross section view of sample I 22 4S OR = 0.5 with processing along the plate to shear tests.

Figure 4.9 shows the wear observed on the first tool. This produced test pieces of types joints 1 and 2 used for metallography, with a total of processings of 2.7 m. In Figure 4.9 B the probe showed practically the shape of a cone with a minimum diameter of 2.2 mm. When the same probe was set at a length of zero is evidenced lack of probe material already consumed for processing (Figure 4.9 B). At higher rotation speeds, with clear evidence of the rotational speed of 2000 rpm, the probe shown an accelerated wear.

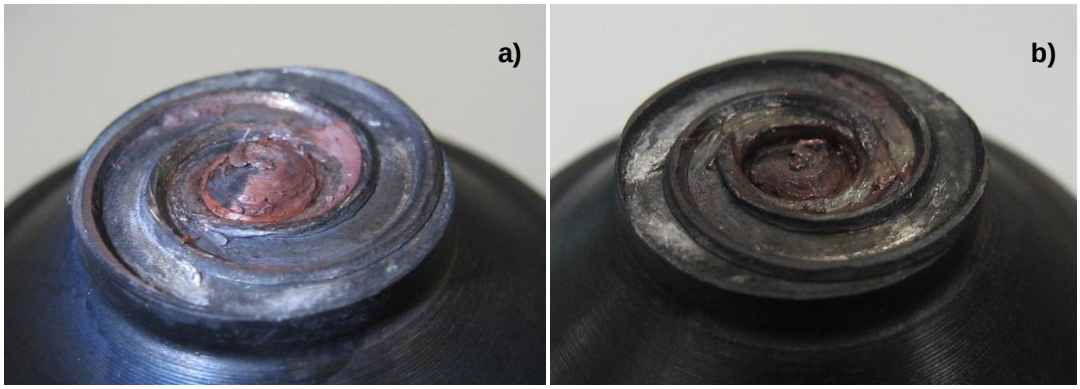

Figure 4.9 – First tool wear after of the samples for metallography on type joints 1 and 2. (a) probe length used of 0.92 mm, (b) probe length equals zero.

The second probe showed wear of the fillets resulting in a minimum diameter of 3.6 mm (Figure 4.10 A). This produced type 1 joints used for shear and bending tests, with a set of processings of 2.0 m. Finally a third probe was used with the same geometries and materials of the above, to processed type 2 joints for shear and bending tests. It was produced a total of 2.0 m processing without apparent of probe wear, as shown in Figure 4.10 B.

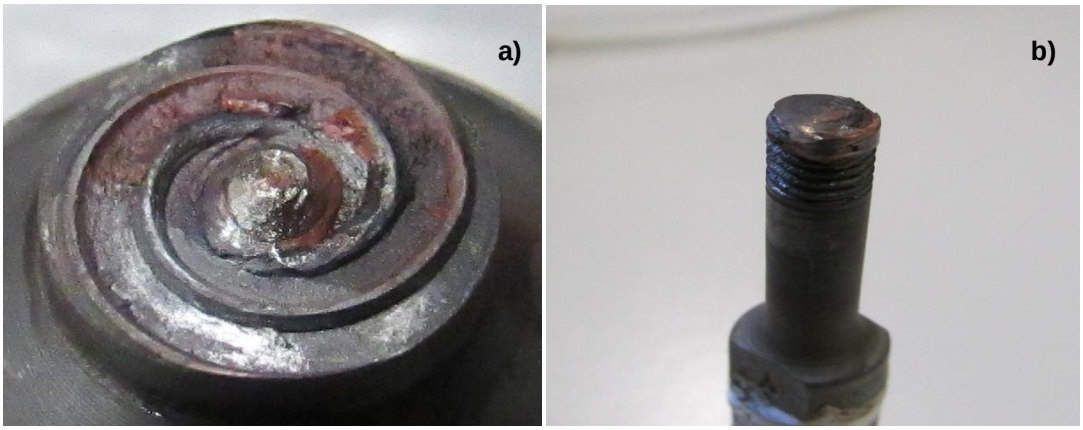

Figure 4.10 - Tool wear after processing of the samples for shear tests and bending tests. (a) Second probe used on type 1 joints, (b) Third probe used on type 2 joints.

4.2.2. **Effect of processing parameters on joined width and surface quality**

Figure 4.11 shows macrographs of samples H12 and H14 indicating the joined width. As the shoulder used had grooves, the processed surfaces of the samples were formed by flash's, which can be seen in more detail in Figure 4:12 B. Samples H 12 and H 14 showed burr in the advance side and a progressive removed of the shoulder on the reverse side without producing burrs. The end of the joined interface in sample H12 can be seen in Figure 4.12 B, as well as a flat interface observed at samples H.

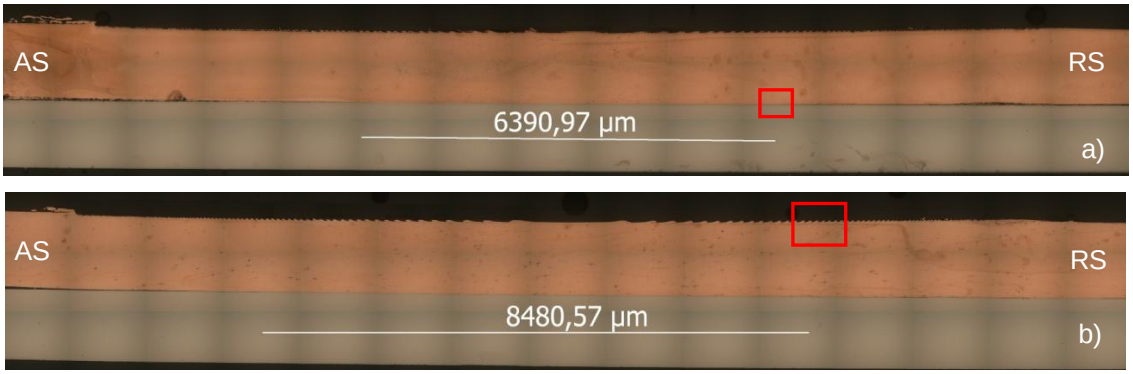

Figure 4.11 – Cross section view with joined width of samples. (a) H 12, (b) H 14.

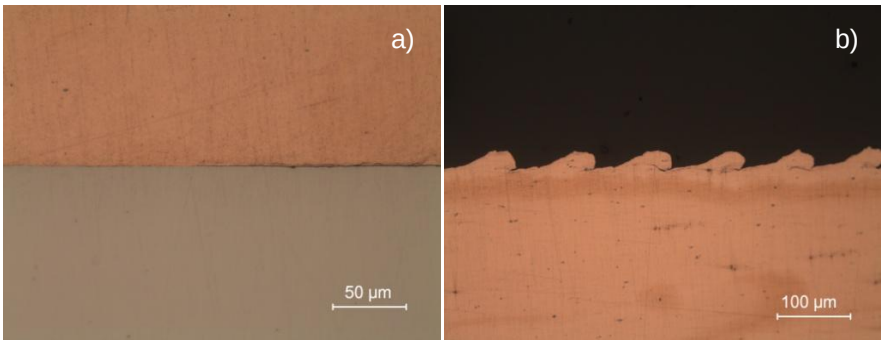

Figure 4.12 – Details of samples. (a) End of joined interface at H 12 sample, (b) Surface flashes on RS at H 14 sample.

In Figure 4.13 A (sample I 18) it is shown a shoulder penetration on the advancing side but without producing burrs, while in the reverse side, the progressive removed of the shoulder did not produced burrs. Unlike observed in the previous samples, type 2 joints were characterized by a surface roughness on stainless steel plate originated from the base material. The wavy surface shows defects as voids in the bottom part with lack of joining (Figure 4.13 B).

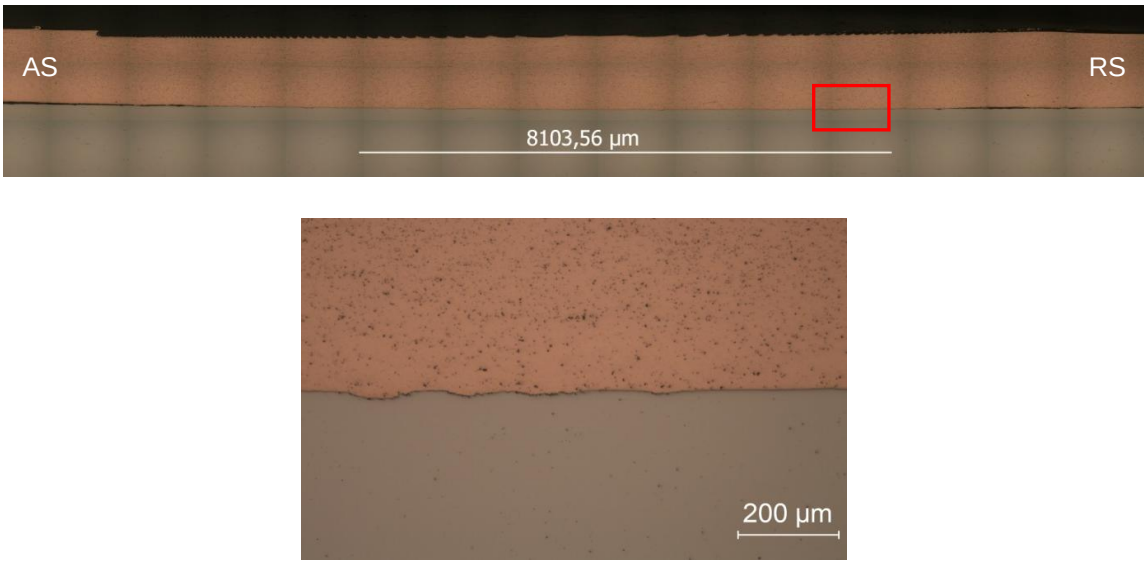

Figure 4.13 – Cross section view of sample I 18. (a) macrography of joint with joined width, (b) details of the joined interface with lack of connection in the cavity.

As mentioned in the previous section, samples produced at higher rotation parameters were more likely to the tool wear. In the Figure 4.14 is presented a macrograph of sample I 29, with a rotation speed of 2000 rpm which produced a high tool wear. In Figure 4.14 B and C are observed details of steel debris due to shoulder wear on the surface and the probe in the processed copper, respectively.

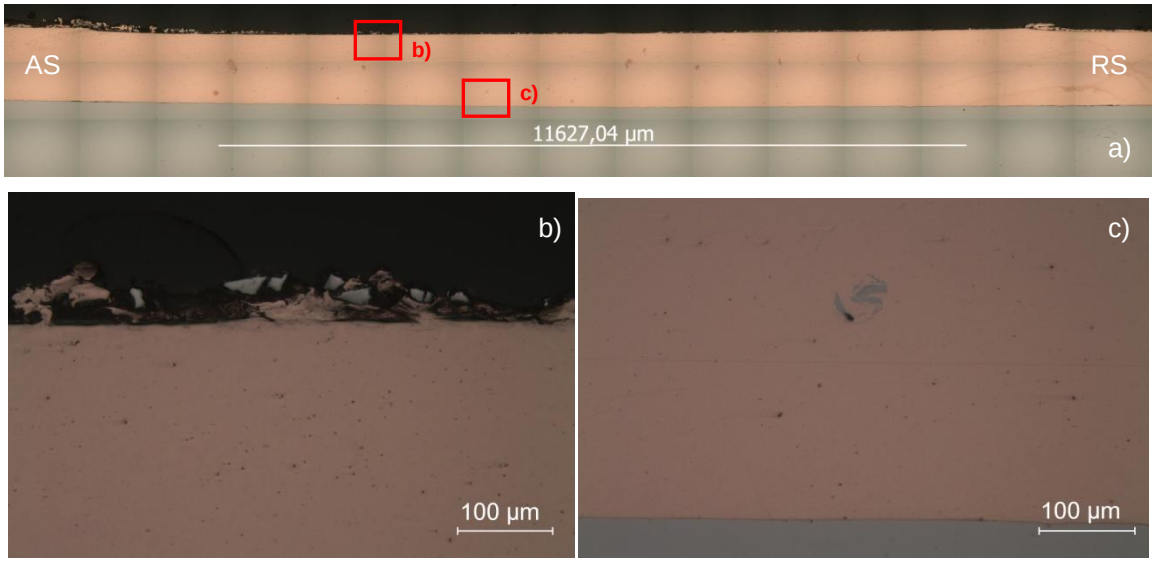

Figure 4.14 – Sample I 29. (a) Macrograph, (b) Detail of the surface showing shoulder wear, (c) Detail of the interface showing probe wear.

Table 4.4 shows the burr location of each sample. It is possible to observe that, comparing to burr formation between different joints, it obtained better results in types 2 joints, having produced joints without burr. Parameters I 18 and I 22 B submitted a shoulder penetration in AS without burr formation.

Table 4.4 - Identification of burr at the AS and the RS for tested samples.

	Type 1 (H)	**Type 2 (I)**
AS / RS free of burr		18, 25, 24, 22, 22 C, 21, 30, 27, 28, 26.
AS fb/ RS wb		22 B.
AS wb/ RS fb	5, 7, 12, 8, 10, 11, 9, 16, 14, 18, 22, 21, 23.	8, 16, 14, 13, 29.
AS / RS with burr	4, 6, 13, 15.	

Joined widths of type 1 joints are summarized in Table 4.5 with a maximum of 10784 µm (joining efficiency = 67.4 %) for parameters of 1600 rev/min and 150 mm/min. Figures 4.15 and 4.16 present the evolution of the joined width with increased rotation and travel speeds, respectively. Although the crossing of trend lines, due to significant differences in the joined area in the beginning and at the end of the plates, Figure 4.15 shows an increasing of joined width as

the rotation speed increases. A lack consistency or trend with increasing travel speed is depicted in Figure 4.16, however this is not true. In order to a correct verification of the travel speed parameter, the processes were distinguished from the Stationary Zone and Near to Edge Zone. Thus there is a clear evidence of a trend for decreasing joined width when increasing the travel speed (Figure 4.17).

Table 4.5 – Joined width of joints type 1 for different rotation and travel speeds with respective sample reference and joining zone (measured in μm).

	Rotation speed (rev/min)			
	1000	1200	1400	1600
Travel speed (mm/min)				
60		6390 (H12, SZ)	9891 (H16, SZ)	-
90	6628 (H4, SZ)	4119 (H8, SZ)	8480 (H14, SZ)	-
120	5920 (H6, SZ)	5524 (H10, SZ)	6064 (H18, SZ)	8317 (H22, SZ)
150	4952 (H7, NtEZ)	8750 (H11, NtEZ)	6744 (H13, NtEZ)	10784 (H21, NtEZ)
180	-	4356 (H9, NtEZ)	3607 (H15, NtEZ)	10305 (H23, NtEZ)

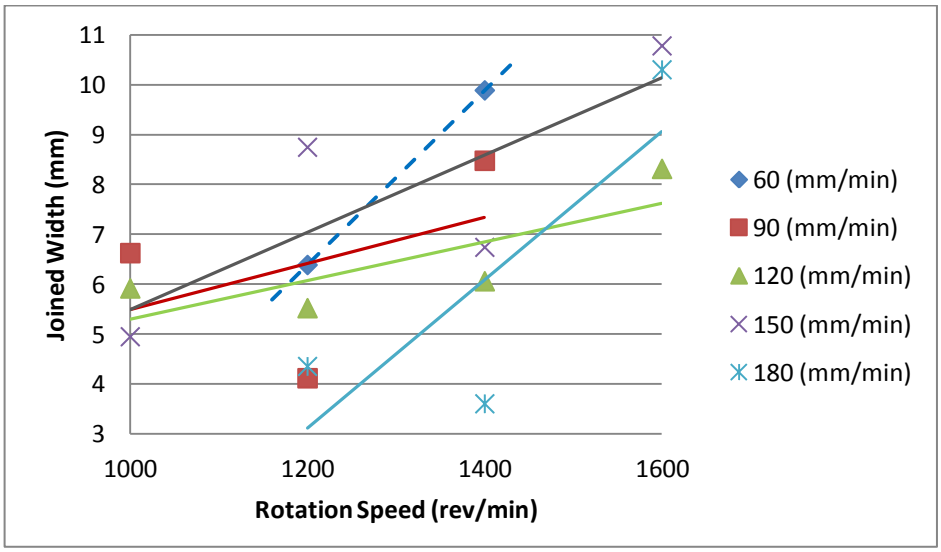

Figure 4.15 - Evolution of joined width with the rotation speed for type 1 joints.

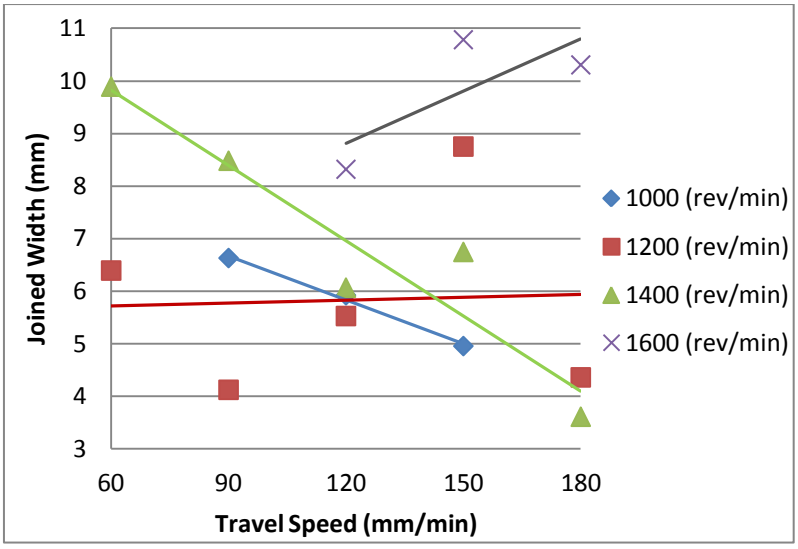

Figure 4.16 - Evolution of joined width with the travel speed for type 1 joints.

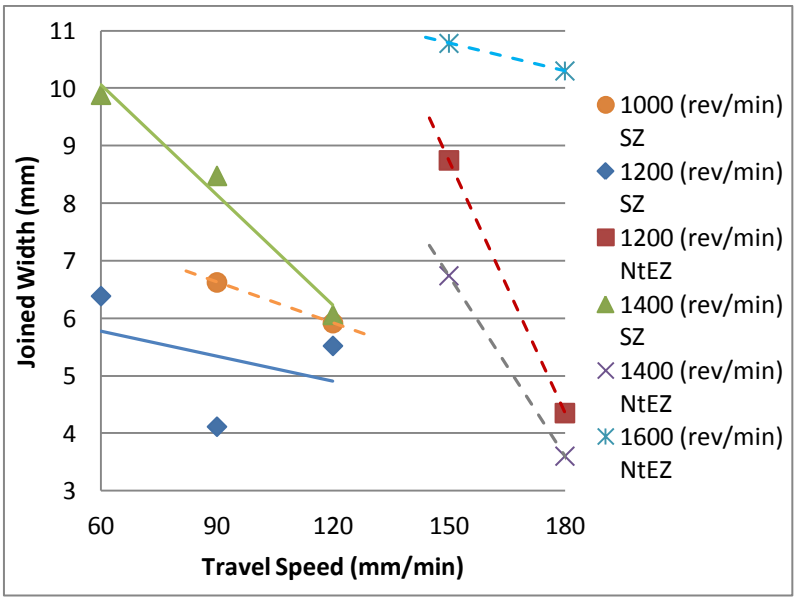

Figure 4.17 - Evolution of joined width with increasing of travel speed at type 1 joints distinguishing processing at the Stationary Zone and Near to Edge Zone.

The joined widths of type 2 joints are summarized in Table 4.6. A maximum of 11813 μm (joining efficiency = 73.8 %) for parameters of 1800 rpm and 90 mm/min was measured. Figures 4.18 and 4.19, as in the previous joints, shows that increasing the rotation speed and decreasing the travel speed, increased the width of the joined interface.

Table 4.6 – Joined width of joints type 2 for different rotation and travel speeds (measured in μm).

	Rotation speed (rpm)				
	1200	1400	1600	1800	2000
Travel speed (mm/min)					
60	-	10412 (I16, SZ)	10933 (I25, SZ)	-	-
90	8406 (I8, NtEZ)	8801 (I14, SZ)	10202 (I24, SZ)	11813 (I30, NtEZ)	-
120	-	8103 (I18, NtEZ)	9504 (I22, SZ)	9029 (I27, SZ)	-
150	-	7754 (I13, NtEZ)	9686 (I21, NtEZ)	10114 (I28, NtEZ)	-
180	-	-	-	9667 (I26, NtEZ)	11627 (I29, NtEZ)

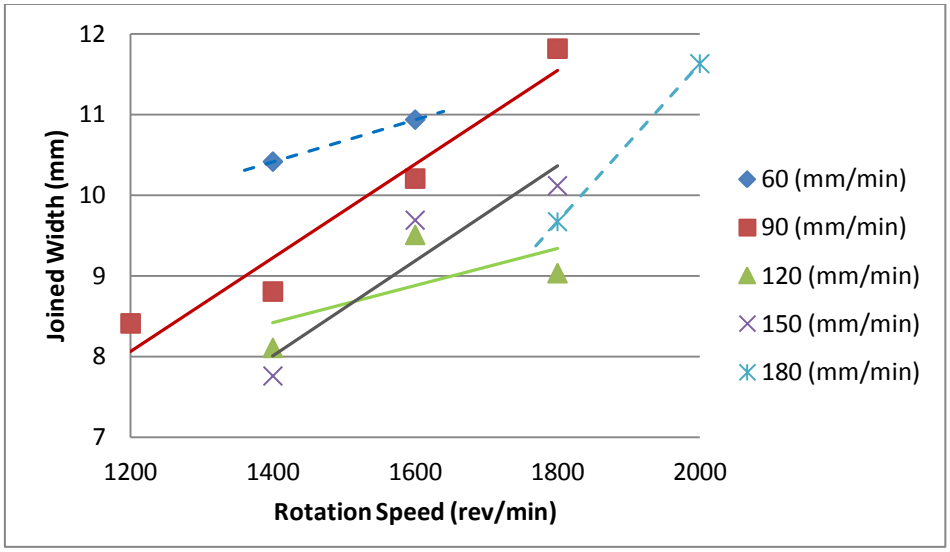

Figure 4.18 - Evolution of joined width with the rotation speed for type 2 joints.

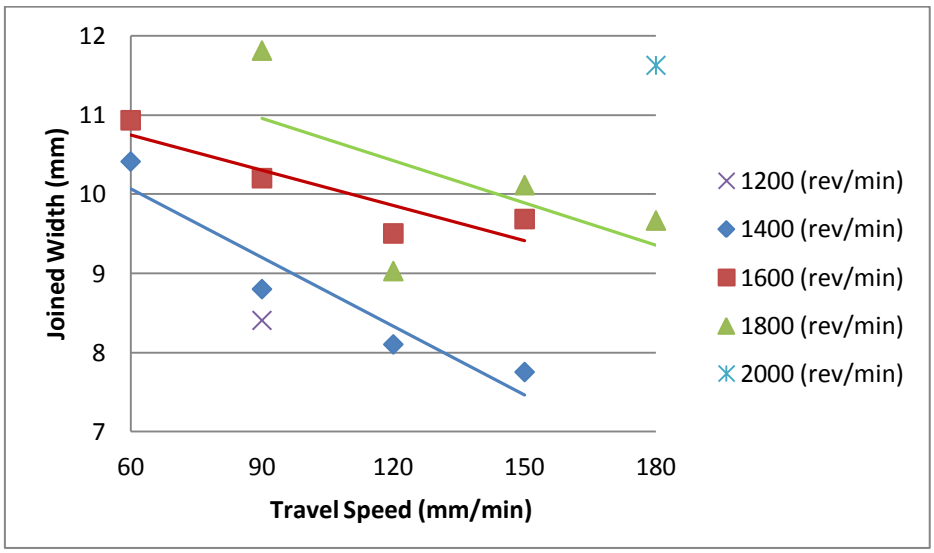

Figure 4.19 - Evolution of joined width with the travel speed for type 2 joints.

When increasing the downward force, a depression on the surface is seen due to the shoulder penetration. In Table 4.7 the sample I 22 B with 6000 N of downward force applied shows a shoulder penetration on both sides, however, only in reverse side presented burr. The remaining samples with 5000 and 5500 N show a progressive penetration of shoulder without burr formation. The joined width measurement of samples indicated that downward force parameters tested were insignificant and reached a maximum variation of 261 microns, insufficient to establish a joined trend.

Table 4.7 – Joined width of joints type 2 for different downward force (measured in μm).

Sample	Df (N)	Macrographs
I 22 C	5000	
I 22	5500	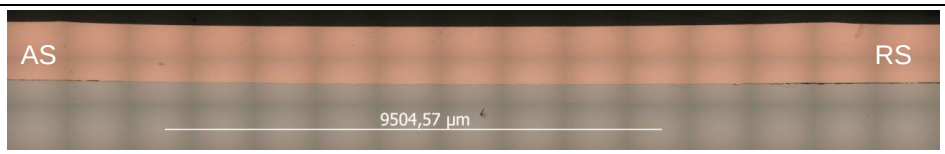
I 22 B	6000	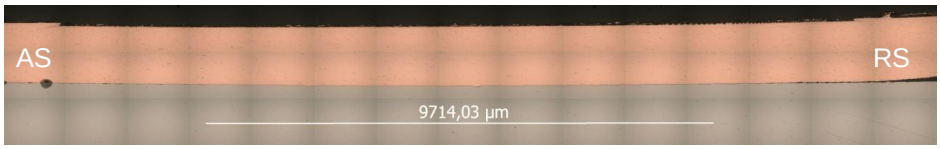

Figure 4.20 shows a macrograph of sample I 22 4S OR = 0.5 with a joined width of 20936 μm. As described above there was a slight burr at the center of the sample caused by the last processing.

Figure 4.20 - Cross section view of sample I 22 4S OR = 0.5.

Observations were made at various sections of chosen joints in order to evaluate the existence of uniform joined width of sample. Three sections per sample, were analyzed separated by about 2 mm (Figure 4.21).

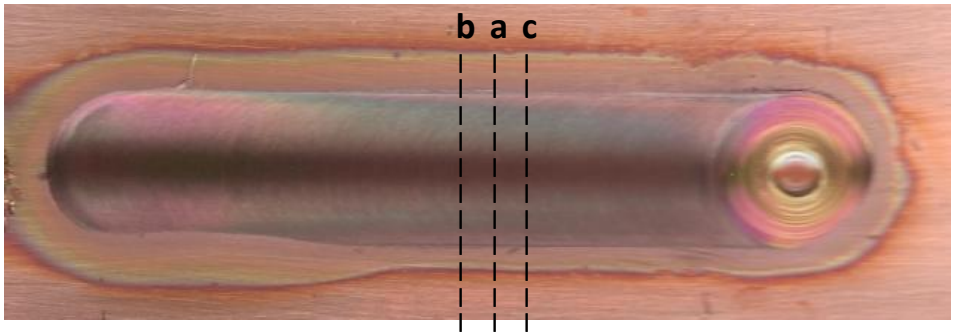

Figure 4.21 - Top view of the processed sample H 21 with the marking of cross section.

Table 4.8 shows sections a, b and c of the sample H 21 which had different joined widths as expected. Table 4.9 summarizes the results of the analyzed samples at joined width and its average and standard deviation. Sample H 21 showed the largest average and standard deviation with 9652 µm and 1418 µm, respectively.

Table 4.8 – Macrograph of the sample H 21 in cross section a, b and c (measured in µm).

Sample	Macrography
H 21 = H 21a	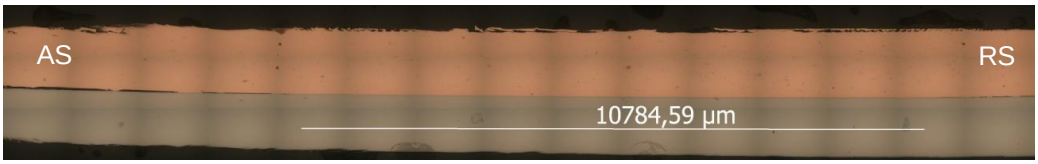
H 21b	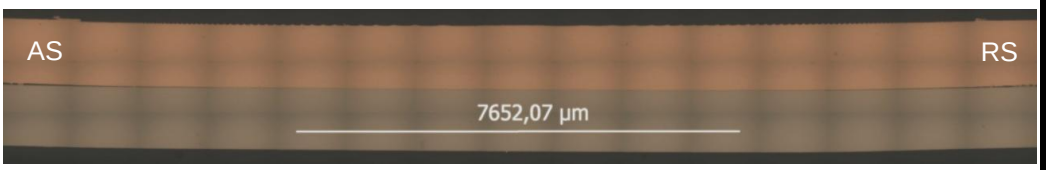
H 21c	

Table 4.9 – Joined width of joints in cross section a, b and c (measured in µm).

Sample	Cross section			Average	Standard deviation
	a	b	c		
H 9	4356		2643	3500	857
H 16	9891	7405	9453	8916	1084
H 22	8317	7270		7794	524
H 21	10784	7652	10519	9652	1418

In Table 4.10 shows the values of joined width for the same processing conditions for joints H and I. This is to compare the width of the joined interface taking into account the difference in thickness of the stainless steel substrate and it can be seen that, in almost all cases, the joined thick in samples I are above these in samples H due to the thickness effect that controls the temperature in the joined region. Table 4.10 shows a maximum variation of 1187 μm.

Table 4.10 – Bonded width in joints H and I (measured in μm).

Sample reference	**Type joints**		**Variation**
	H	I	H - I
16	9891	10412	- 521
14	8480	8801	- 321
13	6744	7754	- 1010
22	8317	9504	- 1187
21	10784	9686	1098

4.2.3. **Structural analysis of the joints**

Table 4.11 presents macrographs of the samples taken for further analysis. The different regions are identified.

The nugget zone is asymmetric and is only present on the copper side. For lower travel speeds such asymmetry tends to decrease, since there was a material flow of lower intensity being pulled. Increasing the rotational speed, it was found an increase in the area caused by the rotational flow of greater intensity that reaches the adjacent areas of the material. Comparing the same parameters on different joints were observed that in the I samples exist less pronounced asymmetry and a higher nugget area. However, this may be due to the use of a threaded probe, which causes a intermittent down flow, tending to vary the asymmetry of the nugget. Table 4.12 indicates the maximum and surface width of the nugget for different parameters tested.

Table 4.11 - Cross section macrographs.

Sample	Parameters	Macrographs
H 16	Ω = 1400 rev/min ϑ_x = 60 mm/min Df = 5500 N $\Omega/\vartheta_x = 23.3$	
H 22	Ω = 1600 rev/min ϑ_x = 120 mm/min Df = 5500 N $\Omega/\vartheta_x = 13.3$	
I 16	Ω = 1400 rev/min ϑ_x = 60 mm/min Df = 5500 N $\Omega/\vartheta_x = 23.3$	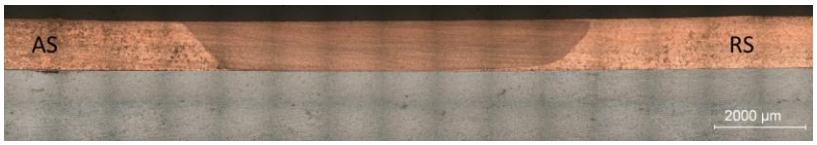
I 25	Ω = 1600 rev/min ϑ_x = 60 mm/min Df = 5500 N $\Omega/\vartheta_x = 26.7$	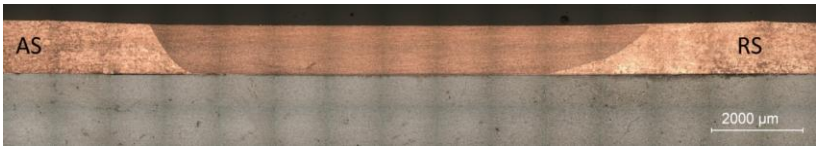
I 22	Ω = 1600 rev/min ϑ_x = 120 mm/min Df = 5500 N $\Omega/\vartheta_x = 13.3$	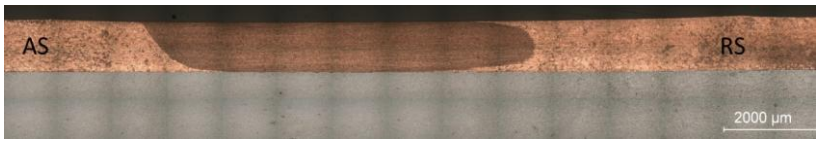

Table 4.12 - Maximum and surface width of the nugget area.

Sample	Maximum width (mm)	Surface width (mm)
H 16	7.3	7.2
H 22	6.1	4.8
I 16	8.9	8.6
I 25	10.8	10.6
I 22	8.0	7.3

Figure 4.22 shows the micrographs of sample H 16 which are very similar to sample H 22. On the copper side it are identified different microstructural zones, due to processing without phase transformation. The nugget zone with fine recrystallized grains, the thermo-mechanically affected zone with deformed grain and a heat affected zone with a grain higher than that of the base material. In the stainless steel, there was no structural modifications since the tool

only entered into the copper, transformations were due to heat conducted across the interface. Sigma phase and precipitation of carbides at grain boundaries were seen, which suggests that the stainless steel has reached a temperature between 650 and 900° C. These are characterized by being brittle and reduce corrosion resistance. In order to avoid these effects it may be placed a plate with high thermal conductivity beneath the substrate to generate a higher heat flow. Another way would be to choose a material with a lower content in carbon or strong carbide formers. Comparing Figure 4.22 E and F, it is clear that there is little sigma phase. Figures 4.22 B1 and G show no change in grain size after FSDP.

Micrographs of sample I 22 are shown in Figure 4.23. On the copper side the same microstructural zones are identified (Figures 4.23 A, B, C and E). The stainless steel showed some differences compared to the previous case. The sigma phase formation and precipitation of carbides at grain boundaries were considerably less and practically nonexistent near the interface, as shown in Figure 4.23 F and D, respectively. This may be due to the increased thickness of the substrate, since it needs more heat to reach the same temperature range of the joints type 1. There was no difference in the formation of sigma phase and precipitation of carbides in relation to the parameters of the different samples contrasted.

Figure 4.24 shows the micrographs of the sample I 22 4S OR = 0.5. The same processing areas on the copper side were identified as described previously, however some differences in the details of the material flow are shown due to multi-steps processing. Figures 4.24 B and D show the material that flows in the following step, denoting a decrease in the bonded area and in the nugget. There was a lack of interpenetration of the nugget as shown in Figure 4:24 C. For complete interpenetration it would be necessary to reduce the overlapping ratio or travel speed. On the stainless steel side, the same effect was seen as in sample I 22, however sigma phase and precipitates were more intense with increasing of distance from the interface (Figure 4.24 F) due to the greater amount of heat generated by multi-step processing. A slight increase in grain size can be identified comparing the microstructures in Figure 4.24 F and H suggesting the effect of heat in the center of the plate.

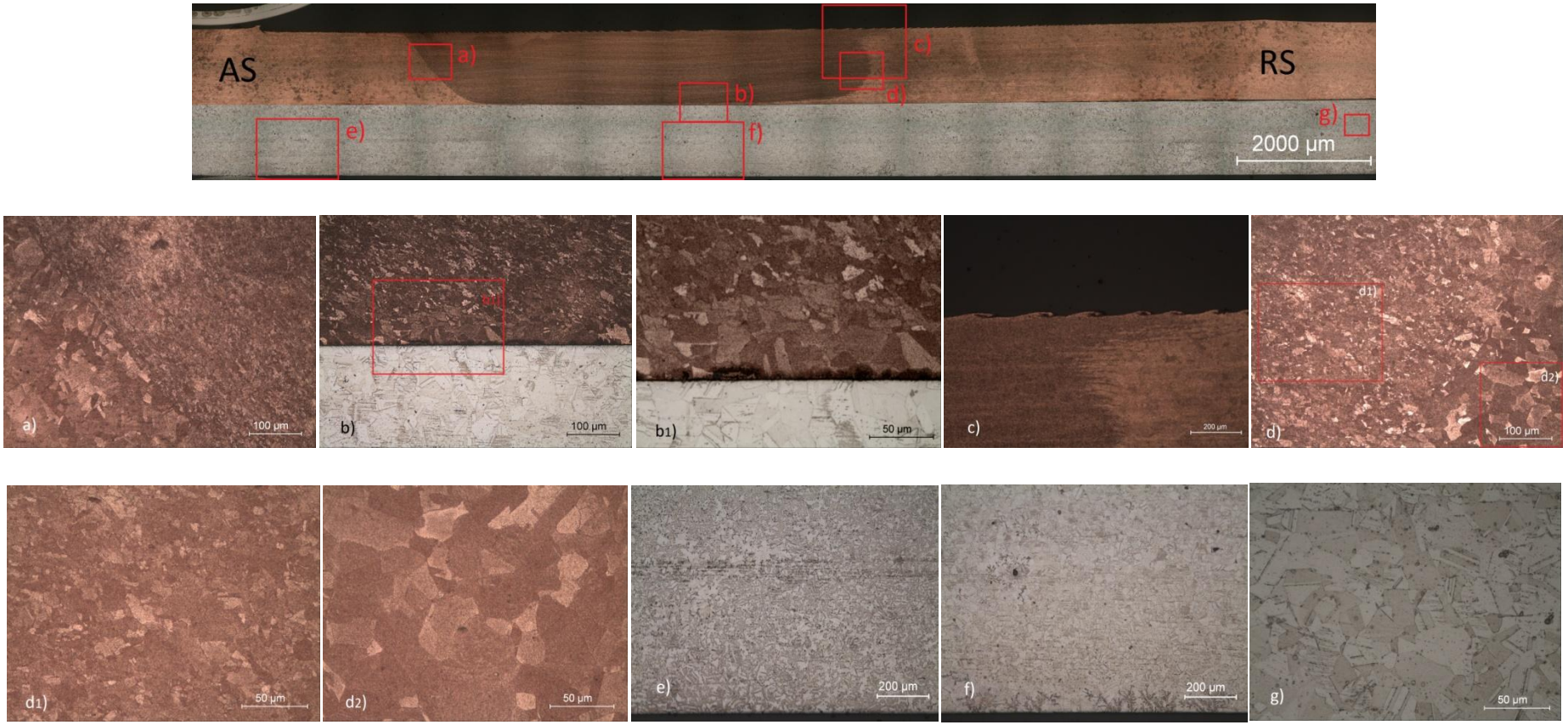

Figure 4.22 - Cross section micrographs of sample H 16. (a) TMAZ and nugget on the AS, (b, b1) interface of the joint, (c) effect of left-hand threaded cylindrical probe and groove shoulder on the TMAZ of RS, (d) TMAZ on the RS, (d1) nugget zone, (d2) HAZ on the RS, (e) occurrence of sigma phase in the limit of processing, (f) occurrence of sigma phase in the middle of processing, (g) Ss outside the processed zone.

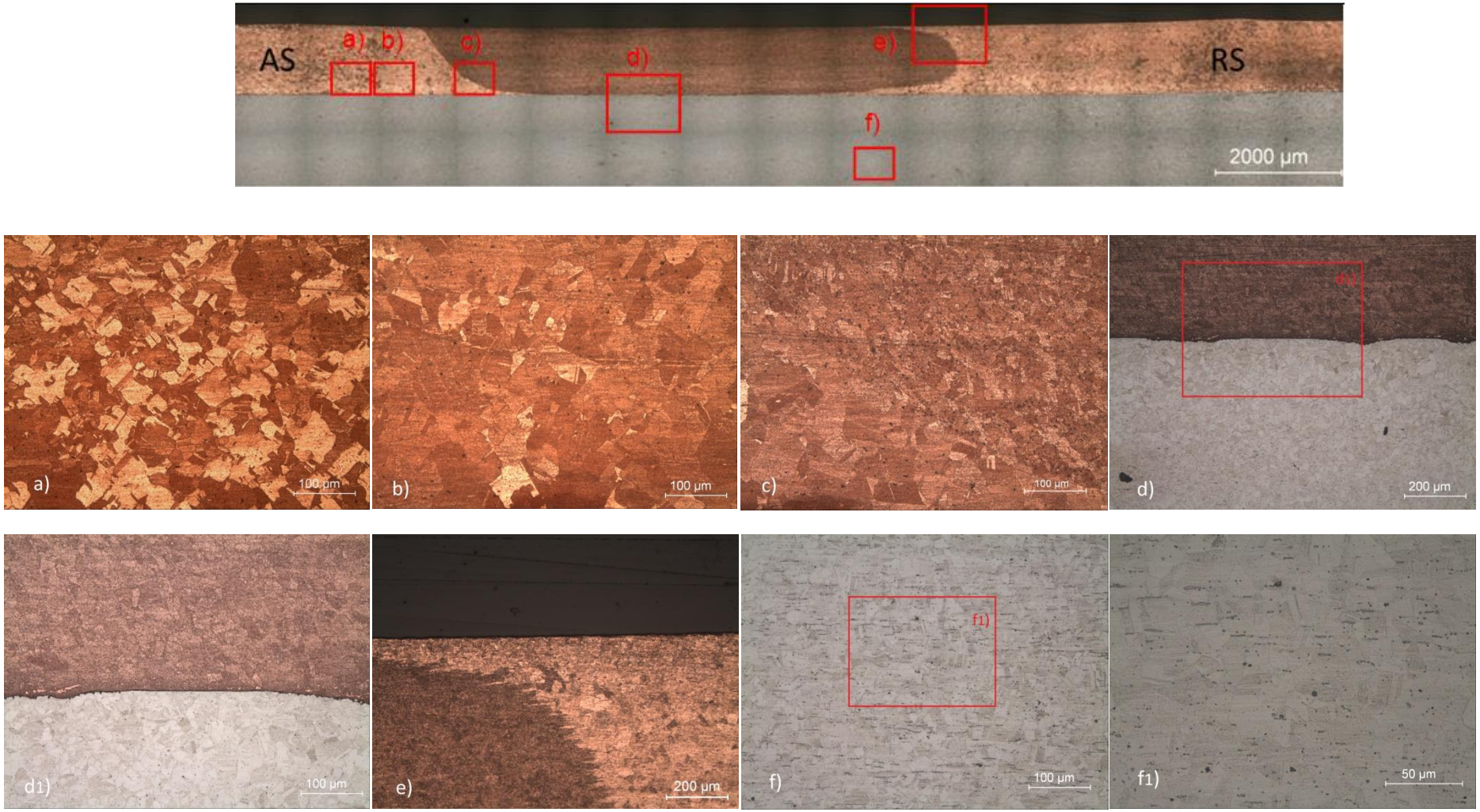

Figure 4.23 - Cross section micrographs of sample I 22. (a) Copper base material, (b) HAZ on the AS, (c) TMAZ and nugget on the AS, (d, d_1) interface of the joint, (e) effect of left-hand threaded cylindrical probe and groove shoulder on the TMAZ of RS, (d) TMAZ on the RS, occurrence of sigma phase in the limit of processing, (f, f_1) occurrence of sigma phase.

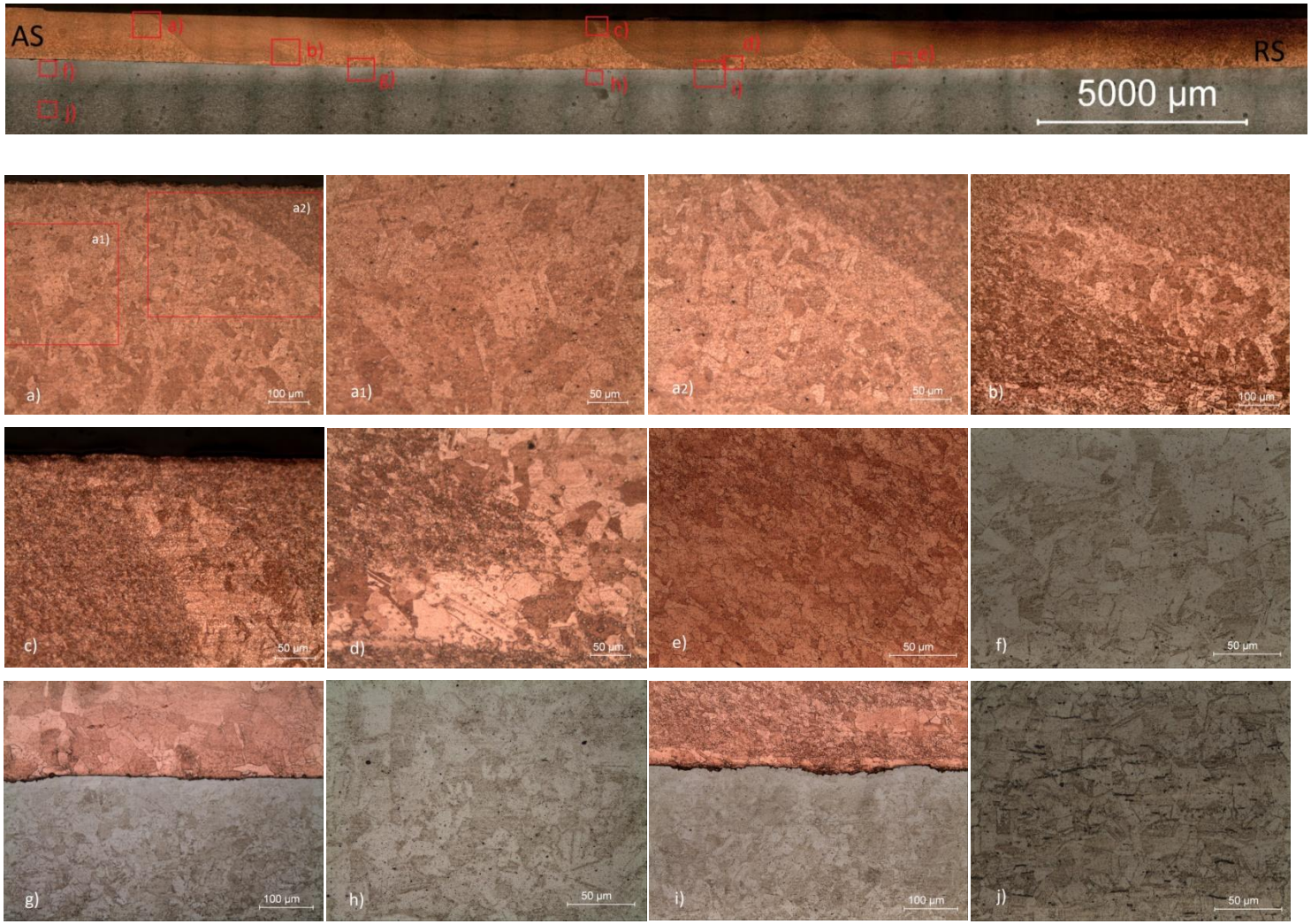

Figure 4.24 - Cross section micrographs of sample I 22 4S OR = 0.5 (a) AS of the first pass, (a1) HAZ; (a2) TMAZ and nugget, (b,d) HAZ and TMAZ at the nugget bottom, (c) overlapped nugget interface, (e) nugget, (f) Ss interface,(g) interface of the joint and HAZ of Cu, (h) Ss interface underneath the processing of copper, (i) interface of the joint with TMAZ and nugget of Cu, (j) Ss with sigma phase presentation.

4.2.4. **SEM/EDS analysis**

To further study the interface SEM with EDS was performed. When analyzing the interface in samples H 16, H 22 and I 25, depicted in Figures 4.25 A, B and C, respectively, extensive voids and defects were seen in sample I 25 and lack of consolidation in sample H 22. Considering the FSDP parameters, hotter joints show less defects, since heat is conducted across the interface establishing a metallic continuity between materials.

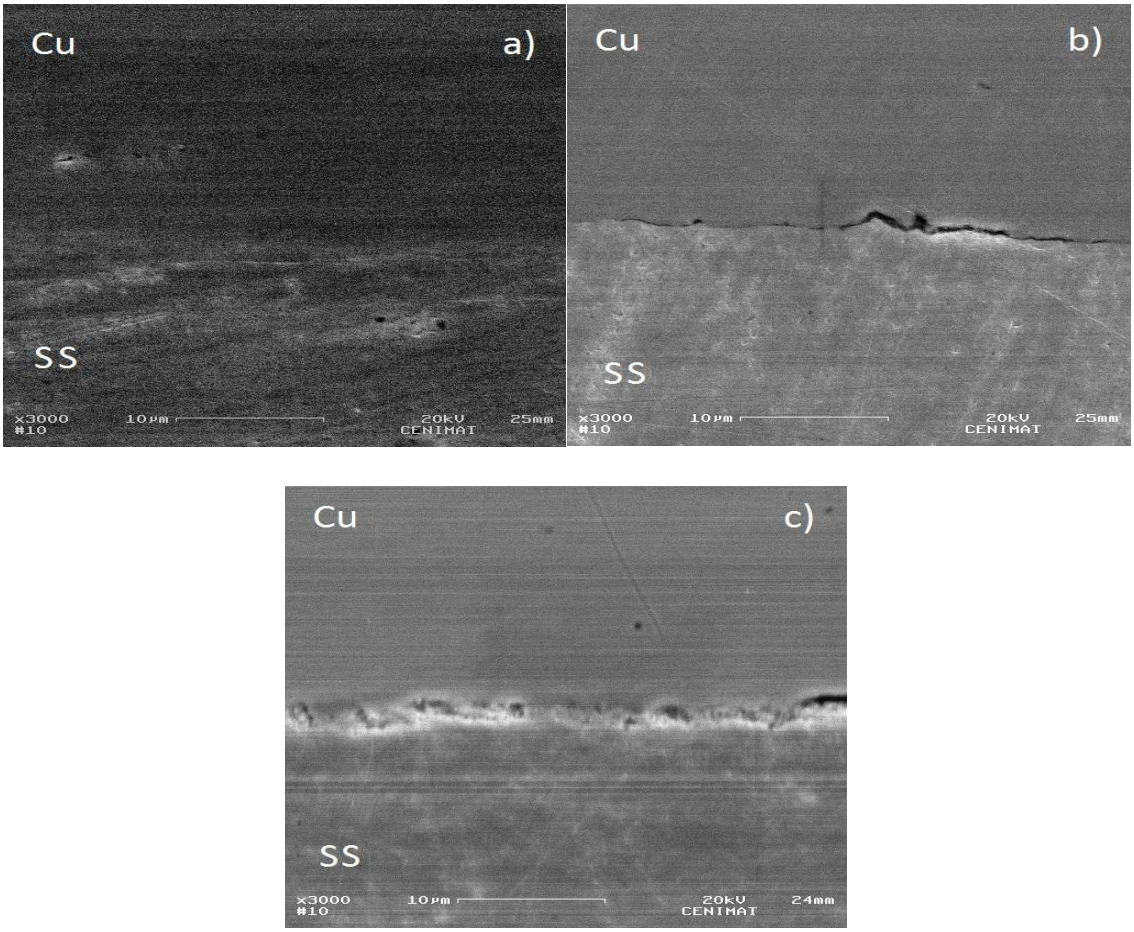

Figure 4.25 – SE image at the interface under center processing. (a) H 16 sample, (b) H 22 sample, (c) I 25 sample.

Observing these regions under back-scattered electron scanning mode, elemental analysis was performed in some points shown in Figure 4.26. Point 1 shows copper while in point 2, Fe, Cr and Ni were identified.

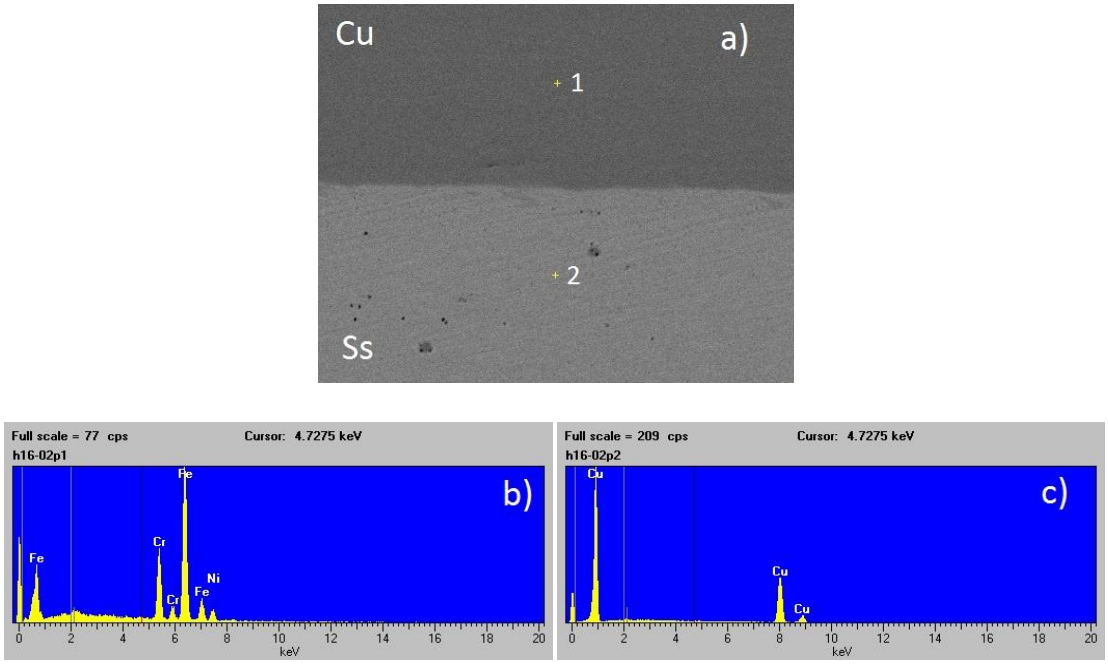

Figure 4.26 – EDS point analysis of H 16 sample. (a) BSE image at the interface under center processing, (b) first position on Cu, (c) second position on Ss.

An analysis was conducted along a line across the interface, as shown in Figure 4.27. Cu, Fe, Ni and Cr were inspected along this line and depicted in B. An IMC layer of 2-3 µm thick was identified, through it was not possible to identify the phases since it needed other techniques for phase identification. Additionally, the resolution of BSE is of 1 to 3 µm thus, there is an incertitude in this IMC identification.

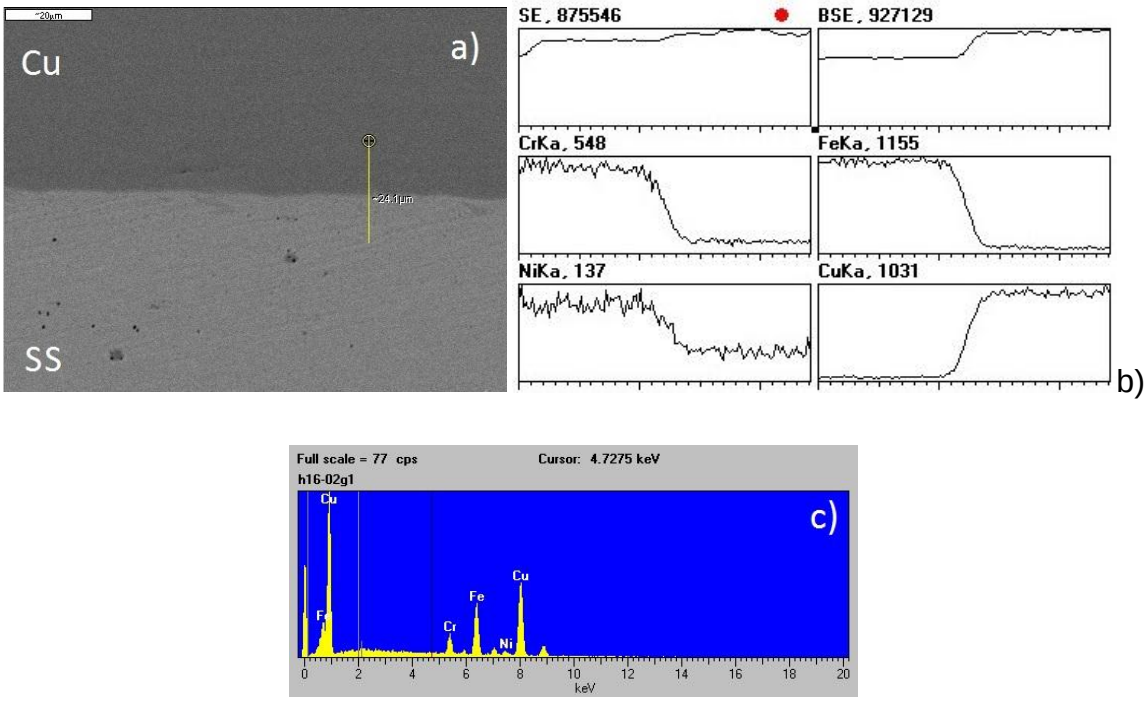

Figure 4.27 - EDS line scanning analysis across the interface of H 16 sample. (a) BSE image at the interface under center processing, (b) variation of the elements along line, (c) elements identified in line.

So, a theoretical analysis was attempted for diffusion in solids (equation 4.1) using the Arrhenius equation [52].

$$D = D_0\, e^{-Q/RT} \tag{4.1}$$

Where:

D is the diffusion coefficient, m^2/s
D_0 is the temperature-independent pre exponential, m^2/s
Q is the activation energy for diffusion, J/mol
R is the gas constant, J/mol.K
T is the absolute temperature, K

Applying the values of the diffusion coefficient and activation energy of copper in gamma iron (FCC) and assuming a temperature of 900 ºC (onset temperature at which the gama iron is stable range), computed D is

$$D = 3 \times 10^{-4}\, e^{-253 \times 10^3/8.314 \times (900 + 273)} \approx 1.62\ \times 10^{-15}\, m^2/s$$

To estimate the thickness of the IMC, equation 4.2 was used where this is the simple solution for second Fick law where x is the distance of diffused atoms, t is the time and D the coefficient calculated above.

$$x = 2\sqrt{D\,t} \tag{4.2}$$

$$x = 2\sqrt{1.62\ \times 10^{-15}\ \times\ 20} \approx 3.60 \times 10^{-7}\, m = 0.36\, \mu m$$

Although estimates of time and temperature set out in the calculation of the distribution are higher than the expectable, the theoretical thickness of this intermediate layer is much lower than the error of the equipment 3 µm. Thus, since the diffusion time and temperature were reduced, the IMC thickness was reduced, not being the SEM/EDS a good technique to measure the IMC thickness for this range of thicknesses.

4.3. Mechanical characterization

This subchapter aim to present results of the mechanical characterization performed, to assess the shear and bending strength, as well as, hardness of the joint. The goal was to analyze the effect of the parameters in joints, taking into account the variation of the downward force, speed of rotation and translation, such as the effect of thickness on the steel plate for the different mechanical tests performed. In hardness tests were performed transverse indentations in the centre of the processing in both materials to analyze parameters effect and indentations parallel to the interface to evaluate the different areas on the copper microstructure. In addition, shear and

bending tests were also analyzed two successive passages in the same position, OR = 1, to observe the joints resistance with higher diffusion applied.

4.3.1. **Hardness tests**

Table 4.13 shows the mean values and standard deviations of base materials.

Table 4.13 – Vickers hardness of base materials.

Vickers Hardness (HV 0.2)			
	Cu (1.1 mm)	Ss (1 mm)	Ss (6 mm)
Average	65.07	184.58	236.18
Standard deviation	± 0.37	± 3.13	± 6.38

Figure 4.28 shows the results of hardness tests performed in the center of processing along the thickness of copper. All tests showed values higher than the hardness of the base material due to metallurgical transformation that lead to decreased grain size of the nugget zone. Type 1 joints (H) show higher hardness values concerning type 2 joints (I) due to a greater concentration of strength in thinner joint. Compared H 16 with I 16 samples had a margin of at least 2.0 HV, whereas H 22 and I 22 had a minimum difference of 3.8 HV. I 16 and I 25 samples had the same travel speed but different rotation speeds. The increase of rotation speed in the sample I 25 led to higher hardness values. The sample I 22 with twice of travel speed and the same rotation speed of I 25 produced a hardness decreasing. This is due to the reduction of time or rotation intensity for metallurgical transformations in the nugget area can occur leading to decreased of grain size. The I 22 B joint with 500 N of downward force increase led to a decrease in hardness, contrary to what would be expected.

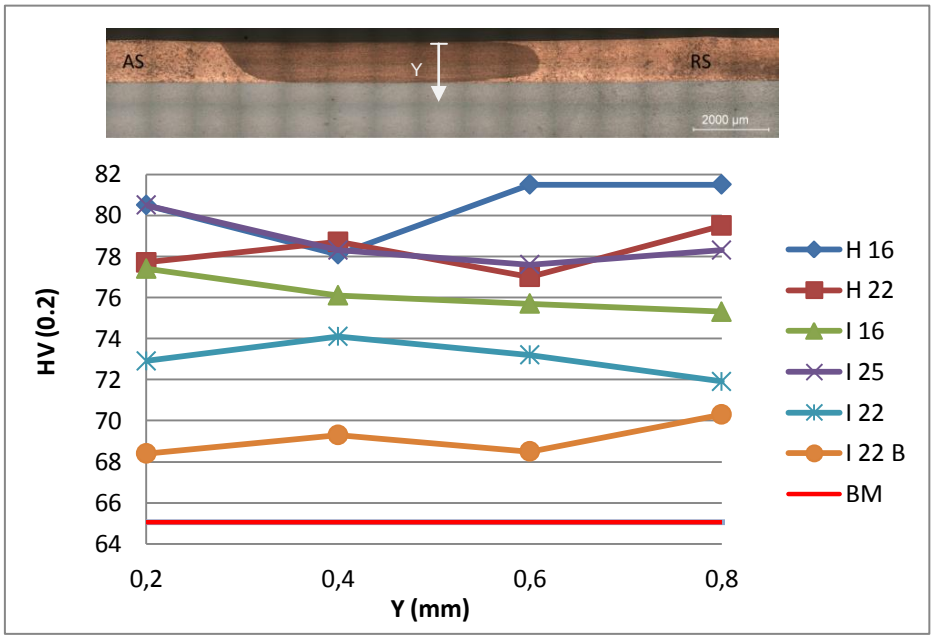

Figure 4.28 - Evolution of hardness transverse profile on copper with varying the parameters (Image example of sample I 22).

Figure 4.29 shows the evolution of hardness transverse profiles on stainless steel. H BM and I BM are presented hardness of the base materials in the thickness of 1 mm and 6 mm. This is in agreement with the micro structural analysis where the fine joints showed high formation of sigma phase, which is brittle and responsible for increased hardness, as opposed to thicker joint in which the sigma phase formation was considerably less and practically nonexistent near the interface. The variation of the parameters did not affect the hardness significantly.

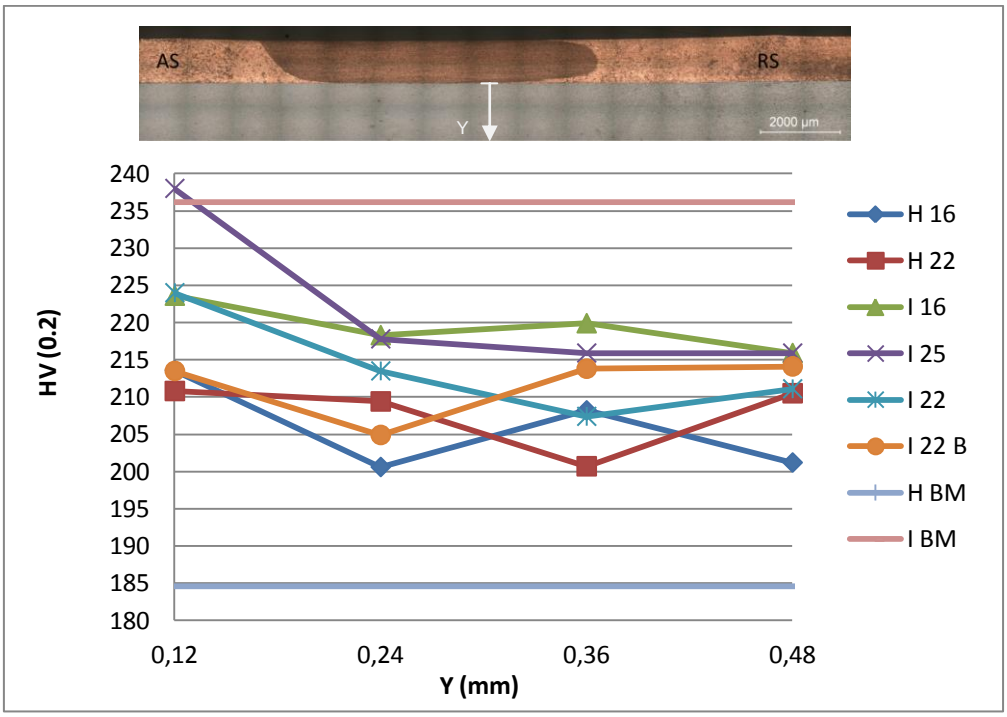

Figure 4.29 – Evolution of hardness transverse profile on stainless steel with varying the parameters (Image example of sample I 22).

An horizontal hardness profile was seen on copper (Figure 4.30). The chosen sample, I 22 showed a average hardness of 13.5% higher than the base material in the nugget zone. In the HAZ in which the grain size was increased, the hardness decreases.

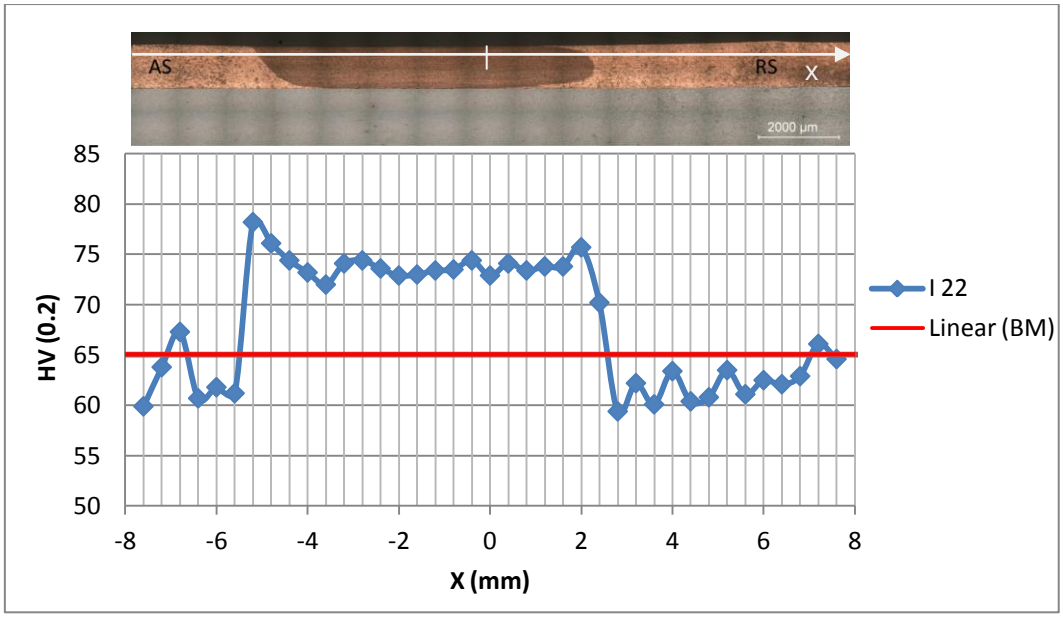

Figure 4.30 - Evolution of the hardness horizontal profile on copper at I 22 sample with respective image.

4.3.2. **Shear tests**

Samples for shear tests were prepared from joints of types 1 and 2.

H 16 and H 22 samples had a ruptured in processing on the reverse side, since this was the largest effort side in the test (Figure 4.31). The joints showed a low necking in copper due to its lower strength compared to SS. Some multi-pass joints, as in samples H 16 2S OR = 1 and H 22 2S OR = 1 showed a non-uniform join during testing some there was no effective joining in these specimens. Stainless steel remained in the elastic regime.

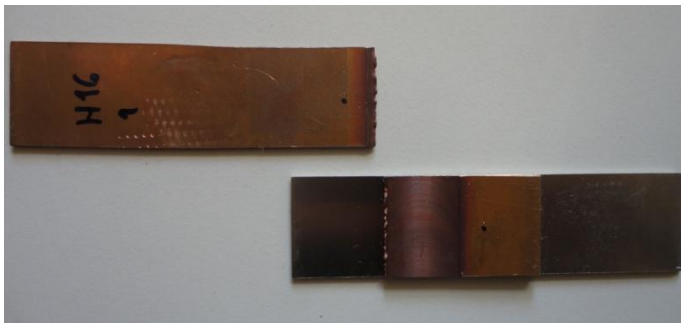

Figure 4.31 - Top view of H 16.1 joint with ruptured in processing on the reverse side.

Shear test curves for type 1 joints are presented in Figure 4.32. Samples H 16 with $\Omega / \vartheta x = 23.3$ ratio greater than H 22 with $\Omega / \vartheta x = 13.3$ ratio, it had higher values of true stress-true strain with a maximum shear strength of the joint that was about 57 % of that of the copper base metal (Figure 4.32 A and B). When two steps with OR = 1 were carried out it was observed tendency to increase the resistance due to increased diffusion time (Figure 4.32 C and D). However this shear resistance greatly varied due to non uniform and continuous joining along the

joint. Specimen 3 of H 22 2S OR = 1 reference achieved a maximum shear strength of the joint that was about 94 % of that of the copper base metal.

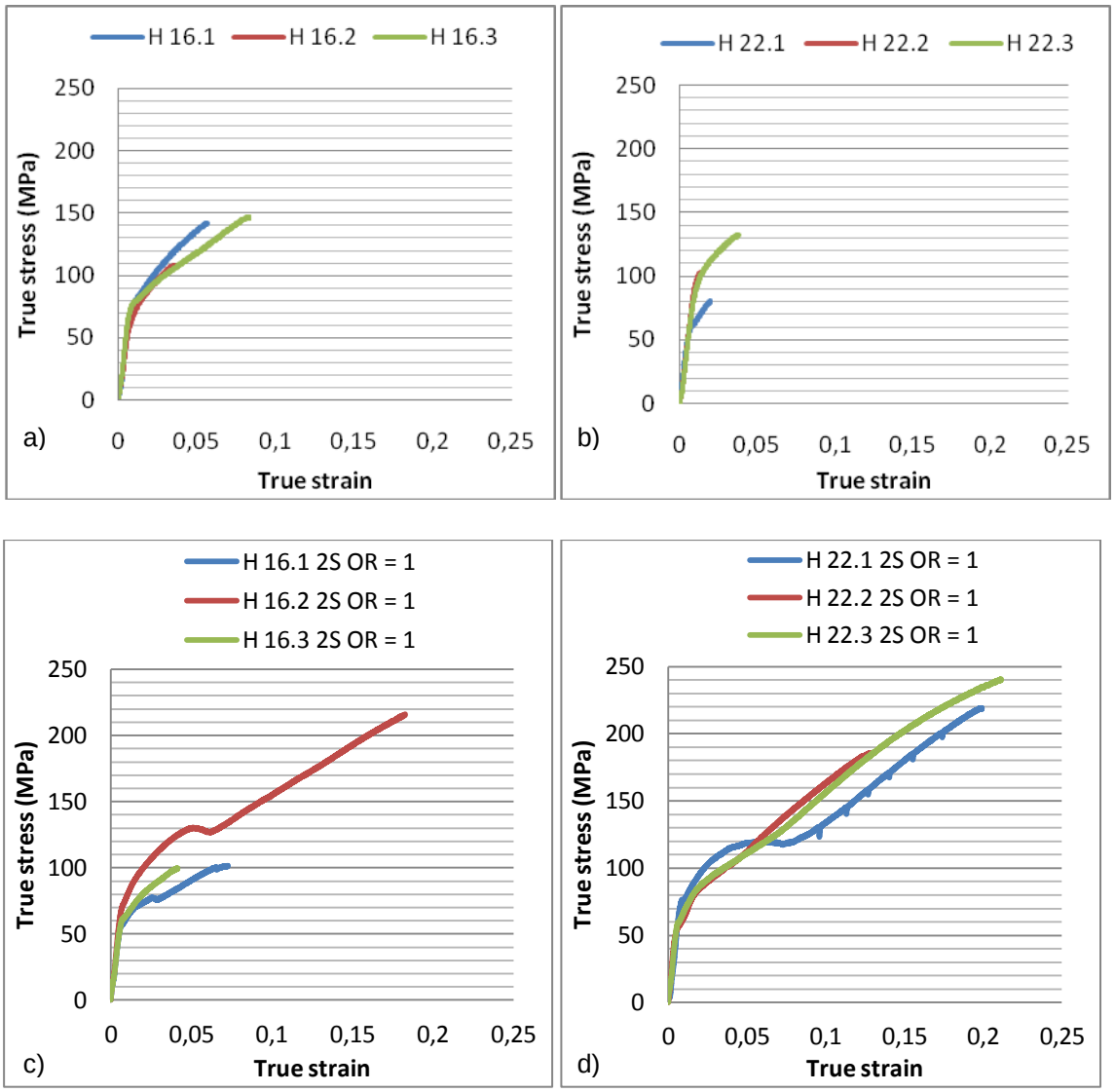

Figure 4.32 – Results of shear testing true stress-true strain curves of type 1 joints. (a) H 16, (b) H 22, (c) H 16 2S OR = 1 and (d) H 22 2S OR = 1.

In joints type 2 an increase in the mechanical resistance was observed when compared to the copper base material of samples I 16, I 22, I 22 B and I 22 4S OR = 0.5, as seen in Figure 4.33. For sample I 25 the fracture occurred along the retreating side in copper, while one specimen suffered decohesion along the bonded length. In Figure 4.33 the samples had a high necking, ductile behavior characteristic of the copper material and the rupture with a 45º crack propagation direction in the base material.

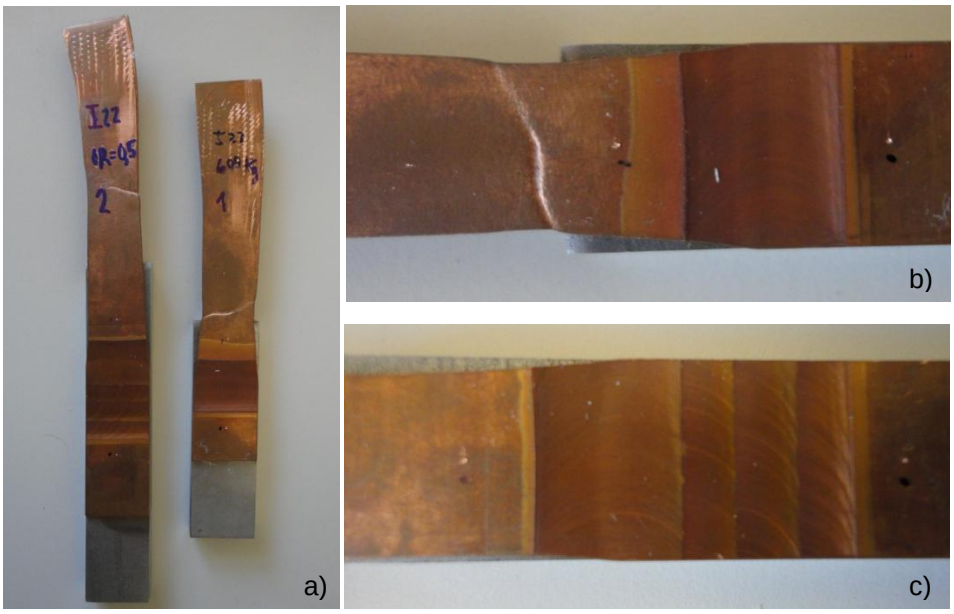

Figure 4.33 - Specimens after shear tests. (a) Top view of I 22 4S OR = 0.5 and I 22 B specimens with ruptured in the base material, (b) Detail of I 22 B specimen, (c) Detail of I 22 4S OR = 0.5 specimen.

The completion of these tests suggests that the choice of parameters that provide greater resistance of joints was a $\Omega / \vartheta x$ ratio between 23.3 and 13.3 (Figure 4.34). The sample I 25, with a ratio of 26.7 provided less resistance than the base material of copper while the minimum ratio threshold may not have been found.

Observing the stress-strain curves, yielding of the joints is observed in some curves due to non uniform joining with good mechanical resistance. When this is not observed, the joints have the same mechanical behaviour has copper base material.

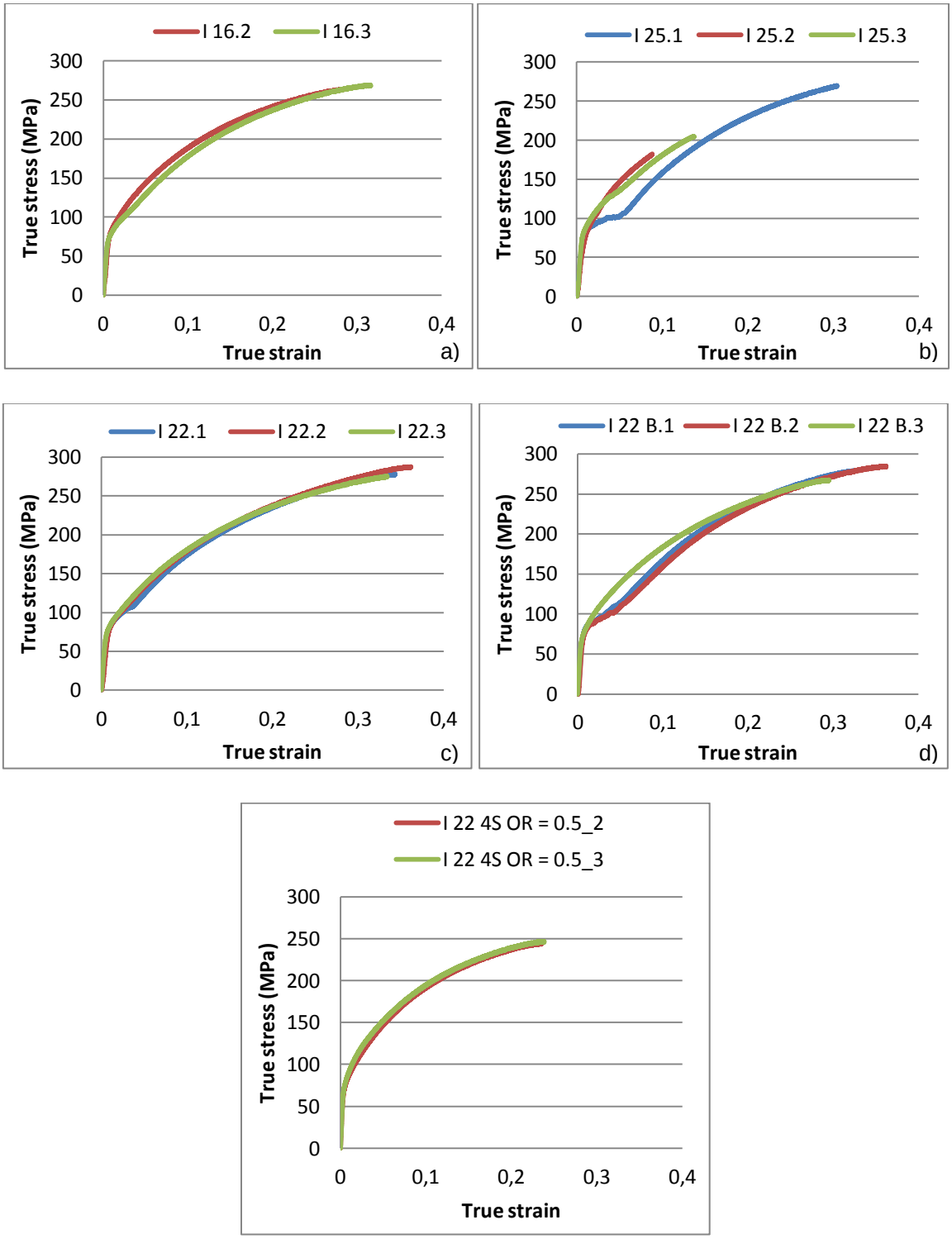

Figure 4.34 – Results of shear testing true stress-true strain curves of type 2 joints. (a) I 16, (b) I 25, (c) I 22, (d) I 22 B and e) I 22 4S OR = 0.5.

4.3.3. **Bending tests**

Three points bending tests were performed on specimens H 16, H 22, H 22 2S OR = 1 of joints type 1 and I 16, I 25, I 22, I 22 4S OR = 0.5 of joints type 2.

Samples I 22.1 4S OR = 0.5 and H 16.2 tested in the bending tests are shown in Figure 4.35. These show an angle of 86 º and 61 º respectively, without visible rupture.

Figure 4.35 - Specimens I 22.1 4S 0R = 0.5 and H 16.2 after bending tests.

Applied forces, displacements and bending angle of the specimens are shown in Figures 4.36 and 4.37.

The maximum forces imposed on the joints type 1 were between 538 and 700 N, as shown in Figure 4.36 A. The first specimens of each parameter were tested for the maximum angle allowed by the specimens support. Samples H 16, H 22 and H 22 2S OR = 1 obtained maximum angles of 93 º, 107 º and 111 º, respectively.

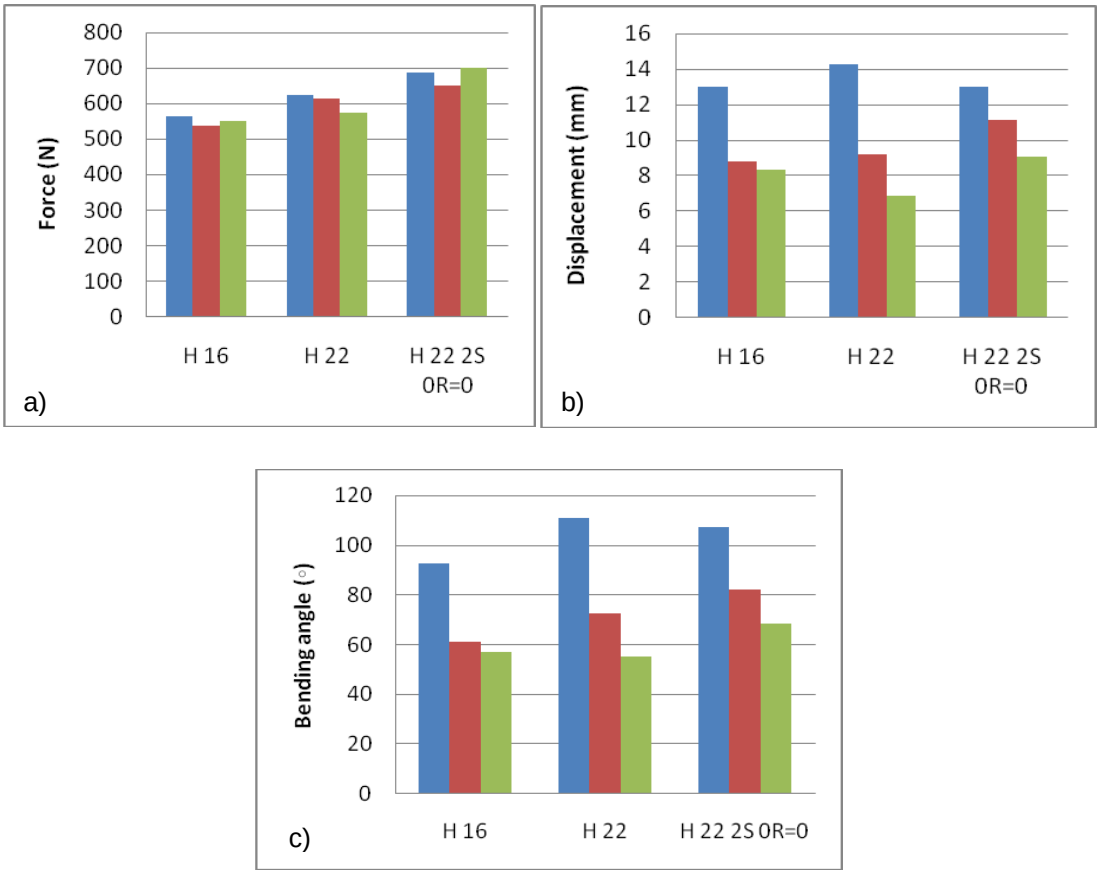

Figure 4.36 – Bending tests results of type 1 joints. (a) Maximum force plot, (b) Maximum displacement plot and (c) Bending angle plot.

Other specimens were testes and showed detachment in joint interface, so these were not considered in this analysis. The force increased substantially due to the increased thickness of stainless steel, reaching a maximum force near 12.5 kN. The second type of joints did not support displacements and bending angles as high as type 1 joints, however sample I 22.1 4S OR = 0.5, with higher bonded area, reached a bending angle of 86 °.

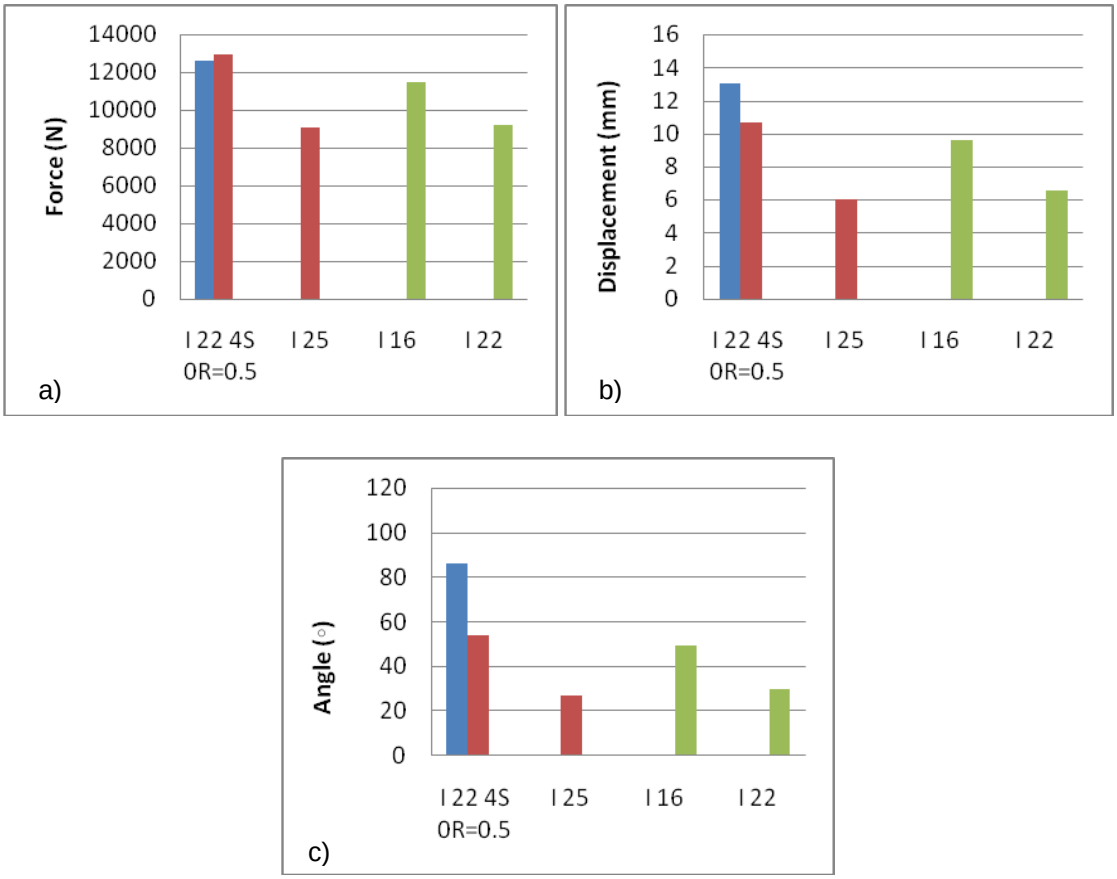

Figure 4.37 – Bending tests results of type 2 joints. (a) Maximum force plot, (b) Maximum displacement plot and (c) Bending angle plot.

4.4. Energy consumption

This subchapter is intended to evaluate the energy consumption in relation to the main parameters of the FSDP. Since this is an essentially a mechanical process control, SCADA files were used which indicate the binary in the z-axis, the distances and the downward force for each instant of time. Vilaça [53] presents the equation 4.3 to establish the mechanical power provided by equipment (P_e) and delivered by the tool during processing of the plates.

$$P_e = \frac{2\pi\Omega}{60} \times T_z + \frac{0.001}{60} \times v_x F_x \tag{4.3}$$

However, Vilaça showed that the energy expended due to the rotation is more than 99% of total energy expended during the process, thus it is possible to approximate to equation 4.4.

$$P_e[W] \approx \frac{2\pi\Omega}{60} \times T_z \tag{4.4}$$

The binary measured during processing (T_z) is the average of the measured binary in the stationary phase of processing.

It was also measured the energy consumption per unit of length (EC_l), where t is the time of processing and $l_{processed}$ is the processed length by the tool, as given by equation 4.5.

$$EC_l\,[J/mm] = P_e\,[W] \times \frac{t\,[s]}{l_{processed}\,[mm]} \tag{4.5}$$

Figures 4.38 at 4.40 were obtained from the Tables D1 to D4 of annex D. The difference in the type of joint did not change significantly the energy consumption.

In Figure 4.38 is observed consumption increases with the increase of the rotation speed, having a minimum consumption (2556 W; 1339 J/mm) for 1000 rpm and maximum (3165 W; 1669 J/mm) for 1600 rpm. Although the torque has decreased, the increase of the rotation is higher.

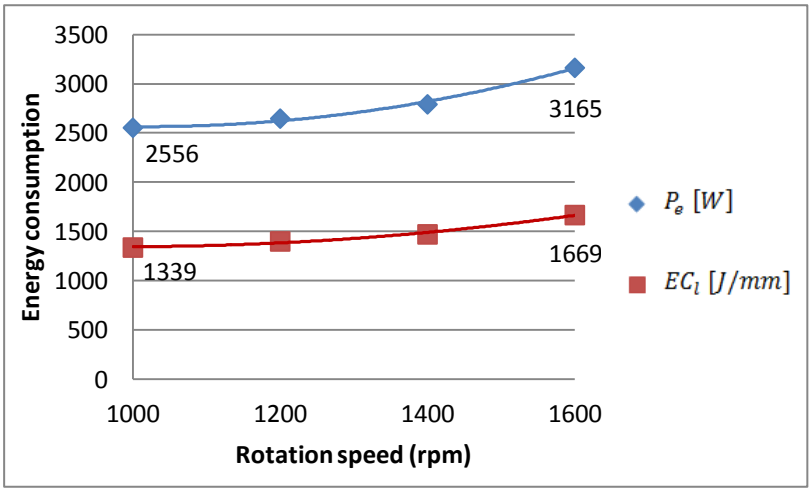

Figure 4.38 - Evolution of energy consumption for different rotation speeds and constant travel speed of 120 mm/min.

The evolution of power consumption for different rotation speeds is shown in Figure 4.39. The power of equipment increased, however at a slower rate when compared with the previous case. To triple the travel speed increases only 233 W. On the other hand, the energy consumption per unit of length follows a declining trend. The increase in travel speed decreased the specific consumption of 2831 J/mm to 1046 J/mm at travel speeds of 60 mm/min to 180 mm/min.

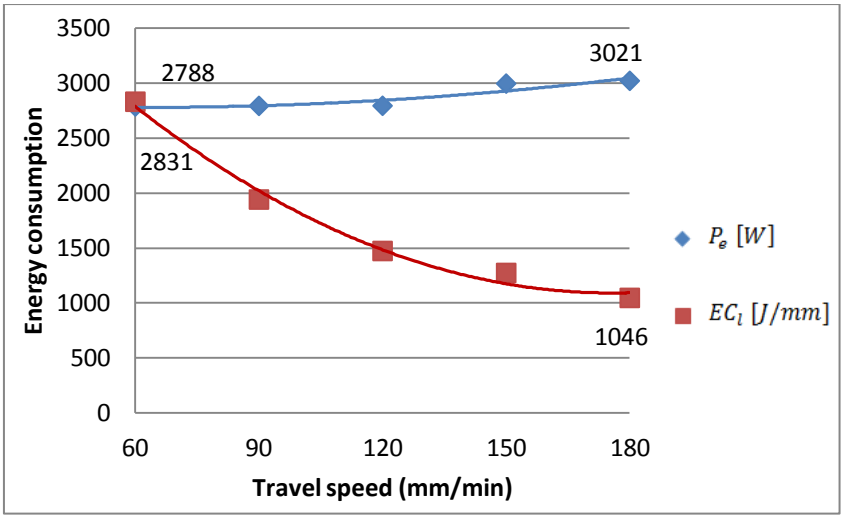

Figure 4.39 - Evolution of energy consumption for different travel speeds and constant rotation speed of 1400 rpm.

As in the analysis of the rotating speed, power consumption increases with the increase of the downward force. A variation of 239 W and 125 J/mm were presented when applied downward forces of 5000 N to 6000 N (Figure 4.40).

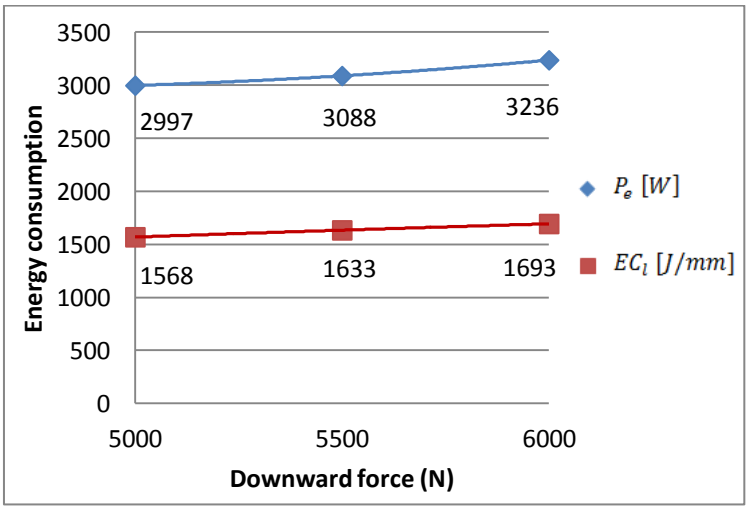

Figure 4.40 - Evolution of energy consumption for different downward forces with constant travel speed of 120 mm/min and rotation speed of 1400 rpm.

5. Final conclusions and suggestions for future work

From the work conducted the following major conclusions can be drawn:

- FSDP proved to be effective in joining copper to stainless steel in the studied thicknesses in lap joint configuration.
- Within the range of parameters tested, for lap joints in Cu 1.1 mm to SS 6 mm thick, the best results in terms of joined width were achieved with the rotation speed of 1800 rpm, travel speed of 90 mm/min and forging force of 5500 N and the joined width was of 11.8 mm (joining efficiency = 73.8 %). For lap joints with similar thickness of Cu to SS of 1 mm thick, lower $\Omega / \vartheta x$ ratios were tested since the necessary heat was lower.
- Surface condition, specially roughness was seen to highly affect the bonded area.
- For the same length processed, the highest wear of the tool was showed on thin joints comparatively with thicker joints due to increased heat concentration.
- Increasing the rotation speed increases the joined width, while this decreases when increasing the travel speed. The forging force has no defined trend, within the parameters tested. Processing near the plate edge increases the joined width due to heat flow boundary conditions.
- There was no mixing between copper and stainless steel in any of the joins produced in the range of parameters testing.
- From a structural point of view, the copper nugget shows an homogeneous fine grain structure, while SS does not exhibit grain size modification, or some grain growth can be identified for multi-pass.
- Nugget area of copper increased with the increase of the rotation speed or decreasing the travel speed.
- The thermo mechanical conditions and time during the FSDP resulted in an interface with diffusion between both materials below 3 μm.
- As far as joint hardness is concerned, it increased in the nugget of copper as expected and increasing $\Omega / \vartheta x$ ratio the hardness increased. In the stainless side, it decreases when compared to the base material for thicker materials and increases for the thinner one. There is no evident correlation between processing parameters and hardness near the interface in SS, which can be explained by the insufficient thermal effect in this material.
- The thicker joints showed ruptures in the base material of copper with a $\Omega / \vartheta x$ ratio between 23.3 and 13.3, while the thin joints showed less resistance.

- High bending angles were measured in thin joints with a maximum of 111 °. The thicker joints exhibited lower bending strength up to 50 º bending angle. When multiple FSDP was performed this increase to 86 ° since the joined width also increased.
- The power consumption per unit of length increases when increasing the rotation speed and the downward force. On the other hand, it decreases when increasing the travel speed.

As suggestions for future work the following have been identified:

- Use different probe geometries specially threaded ones to increase the material flow downwards and improve joining.
- Study of the evolution of heat during processing.
- Perform corrosion tests to evaluate the joined material behavior.
- Study the interface by other techniques, as transmission electron microscopy and x-ray diffraction to identify existing phases.
- Study quantitatively the effect of surface roughness on the FSDP.
- Study the edge effect since heat and mass flow are different when joining close to the free surface of a component.

6. References

[1] T. Ogura, Y. Saito, T. Nishida, H. Nishida, T. Yoshida, N. Omichi, M. Fujimoto, and A. Hirose, "Partitioning evaluation of mechanical properties and the interfacial microstructure in a friction stir welded aluminum alloy/stainless steel lap joint," *Scripta Materialia,* vol. 66, pp. 531-534, Apr 2012.

[2] M. I. Barrena, J. M. G. de Salazar, and L. Matesanz, "Interfacial microstructure and mechanical strength of WC-Co/90MnCrV8 cold work tool steel diffusion bonded joint with Cu/Ni electroplated interlayer," *Materials & Design,* vol. 31, pp. 3389-3394, Aug 2010.

[3] T. F. Kong, L. C. Chan, and T. C. Lee, "Qualitative study of bimetallic joints produced by solid state welding process," *Science and Technology of Welding and Joining,* vol. 13, pp. 679-682, Nov 2008.

[4] T. F. Kong, L. C. Chan, and T. C. Lee, "Experimental Study of Effects of Process Parameters in Forge-Welding Bimetallic Materials: AISI 316L Stainless Steel and 6063 Aluminium Alloy," *Strain,* vol. 45, pp. 373-379, Aug 2009.

[5] N. Orhan, M. Aksoy, and M. Eroglu, "A new model for diffusion bonding and its application to duplex alloys," *Materials Science and Engineering a-Structural Materials Properties Microstructure and Processing,* vol. 271, pp. 458-468, Nov 1999.

[6] S. Saravanan and K. Raghukandan, "Weldability Windows for Dissimilar Metals Cladding Using Explosives," *Theory and Practice of Energetic Materials, Vol Viii,* pp. 585-589, 2009.

[7] W. U. Syed, A. J. Pinkerton, Z. Liu, and L. Li, "Coincident wire and powder deposition by laser to form compositionally graded material," *Surface & Coatings Technology,* vol. 201, pp. 7083-7091, May 2007.

[8] O. Yilmaz and H. Celik, "Electrical and thermal properties of the interface at diffusion-bonded and soldered 304 stainless steel and copper bimetal," *Journal of Materials Processing Technology,* vol. 141, pp. 67-76, Oct 2003.

[9] R. K. Roy, S. Singh, M. K. Gunjan, A. K. Panda and A. Mitra, "Joining of 304SS and pure copper by rapidly solidified Cu-based braze alloy," *Fusion Engineering and Design*, vol. 86, pp. 452-455, Jun 2011.

[10] H. Sabetghadam, A. Z. Hanzaki, and A. Araee, "Diffusion bonding of 410 stainless steel to copper using a nickel interlayer," *Materials Characterization,* vol. 61, pp. 626-634, Jun 2010.

[11] J. T. Xiong, Q. Xie, J. L. Li, F. S. Zhang, and W. D. Huang, "Diffusion Bonding of Stainless Steel to Copper with Tin Bronze and Gold Interlayers," *Journal of Materials Engineering and Performance,* vol. 21, pp. 33-37, Jan 2012.

[12] N. T. Kumbhar, S. K. Sahoo, I. Samajdar, G. K. Dey, and K. Bhanumurthy, "Microstructure and microtextural studies of friction stir welded aluminium alloy 5052," *Materials & Design,* vol. 32, pp. 1657-1666, Mar 2011.

[13] W. U. H. Syed, A. J. Pinkerton, Z. Liu, and L. Li, "Single-step laser deposition of functionally graded coating by dual 'wire-powder' or 'powder-powder' feeding - A comparative study," *Applied Surface Science,* vol. 253, pp. 7926-7931, Jul 2007.

[14] H. Yan, P. L. Zhang, Z. S. Yu, C. G. Li, and R. D. Li, "Development and characterization of laser surface cladding (Ti,W)C reinforced Ni-30Cu alloy composite coating on copper," *Optics and Laser Technology,* vol. 44, pp. 1351-1358, Jul 2012.

[15] S. Sato, T. Kuroda, T. Kurasawa, K. Furuya, I. Togami, and H. Takatsu, "Mechanical properties of HIP bonded joints of austenitic stainless steel and Cu-alloy for fusion experimental reactor blanket," *Journal of Nuclear Materials,* vol. 233, pp. 940-944, Oct 1996.

[16] A. D. Ivanov, S. Sato, and G. Le Marois, "Evaluation of hot isostatic pressing for joining of fusion reactor structural components," *Journal of Nuclear Materials,* vol. 283, pp. 35-42, Dec 2000.

[17] WTIA: Welding Technology Institute of Australia. (2006, 03 Jul 2012). *HOT ISOSTATIC PRESSING (HIP) FOR MANUFACTURE OF ORTHOPAEDIC IMPLANTS*. Available: http://www.wtia.com.au/pdf/TGN-MS-01%20HIP.pdf

[18] S. H. Goods and J. D. Puskar, "Solid state bonding of CuCrZr to 316L stainless steel for ITER applications," *Fusion Engineering and Design,* vol. 86, pp. 1634-1638, Oct 2011.

[19] G. LeMarois, C. Dellis, J. M. Gentzbittel, and F. Moret, "HIP'ing of copper alloys to stainless steel," *Journal of Nuclear Materials,* vol. 233, pp. 927-931, Oct 1996.
[20] K. Raghukandan, "Analysis of the explosive cladding of cu-low carbon steel plates," *Journal of Materials Processing Technology,* vol. 139, pp. 573-577, Aug 2003.
[21] F. Findik, "Recent developments in explosive welding," *Materials & Design,* vol. 32, pp. 1081-1093, Mar 2011.
[22] A. Durgutlu, H. Okuyucu, and B. Gulenc, "Investigation of effect of the stand-off distance on interface characteristics of explosively welded copper and stainless steel," *Materials & Design,* vol. 29, pp. 1480-1484, 2008.
[23] M. J. Fernandus, T. Senthilkumar, and V. Balasubramanian, "Developing Temperature-Time and Pressure-Time diagrams for diffusion bonding AZ80 magnesium and AA6061 aluminium alloys," *Materials & Design,* vol. 32, pp. 1651-1656, Mar 2011.
[24] M. J. Fernandus, T. Senthilkumar, V. Balasubramanian, and S. Rajakumar, "Optimising diffusion bonding parameters to maximize the strength of AA6061 aluminium and AZ31B magnesium alloy joints," *Materials & Design,* vol. 33, pp. 31-41, Jan 2012.
[25] K. Bhanumurthy, R. K. Fotedar, D. Joyson, G. B. Kale, A. L. Pappachan, A. K. Grover, and J. Krishnan, "Development of tubular transition joints of aluminium/stainless steel by deformation diffusion bonding," *Materials Science and Technology,* vol. 22, pp. 321-330, Mar 2006.
[26] O. Yilmaz and M. Aksoy, "Investigation of micro-crack occurrence conditions in diffusion bonded Cu-304 stainless steel couple," *Journal of Materials Processing Technology,* vol. 121, pp. 136-142, Feb 14 2002.
[27] H. Nishi, T. Araki, and M. Eto, "Diffusion bonding of alumina dispersion-strengthened copper to 316 stainless steel with interlayer metals," *Fusion Engineering and Design,* vol. 39-40, pp. 505-511, Sep 1998.
[28] H. Sabetghadam, A. Z. Hanzaki, A. Araee, and A. Hadian, "Microstructural Evaluation of 410 SS/Cu Diffusion-Bonded Joint," *Journal of Materials Science & Technology,* vol. 26, pp. 163-169, Feb 2010.
[29] I. S. Batra, G. B. Kale, T. K. Saha, A. K. Ray, J. Derose, and J. Krishnan, "Diffusion bonding of a Cu-Cr-Zr alloy to stainless steel and tungsten using nickel as an interlayer," *Materials Science and Engineering a-Structural Materials Properties Microstructure and Processing,* vol. 369, pp. 119-123, Mar 25 2004.
[30] R. S. Mishra and Z. Y. Ma, "Friction stir welding and processing," *Materials Science & Engineering R-Reports,* vol. 50, pp. 1-78, Aug 31 2005.
[31] Z. Y. Ma, "Friction stir processing technology: A review," *Metallurgical and Materials Transactions a-Physical Metallurgy and Materials Science,* vol. 39A, pp. 642-658, Mar 2008.
[32] J. P. M. Gandra, "Preliminary Study on the Production of Functionally Graded Materials by Friction Stir Processing," Mestre em Engenharia Mecânica, Departamento de Engenharia Mecânica e Industrial, Universidade Nova de Lisboa - Faculdade de Ciências e tecnologia, Lisboa, 2010.
[33] P. L. Threadgill, A. J. Leonard, H. R. Shercliff, and P. J. Withers. (2009, 30 Jun 2012). *Friction stir welding of aluminium alloys*. Available: http://www.twi.co.uk/technical-knowledge/published-papers/friction-stir-welding-of-aluminium-alloys/
[34] P. L. Threadgill, "Terminology in friction stir welding," *Science and Technology of Welding and Joining,* vol. 12, pp. 357-360, Jul 2007.
[35] H. Fujii, L. Cui, M. Maeda, and K. Nogi, "Effect of tool shape on mechanical properties and microstructure of friction stir welded aluminum alloys," *Materials Science and Engineering a-Structural Materials Properties Microstructure and Processing,* vol. 419, pp. 25-31, Mar 15 2006.
[36] R. Rai, A. De, H. K. D. H. Bhadeshia, and T. DebRoy, "Review: friction stir welding tools," *Science and Technology of Welding and Joining,* vol. 16, pp. 325-342, May 2011.
[37] P. A. Colegrove and P. L. Threadgill. (2003, 30 Jun 2012). *Development of the Trivex(TM) Friction Stir Welding Tool*. Available: http://www.twi.co.uk/technical-knowledge/published-papers/development-of-the-trivextm-friction-stir-welding-tool-february-2003/?locale=en
[38] S. W. Kallee, E. D. Nicholas, and W. M. Thomas. (2001, 30 Jun 2012). *Friction stir welding - invention, innovations and applications*. Available:

http://www.twi.co.uk/technical-knowledge/published-papers/friction-stir-welding-invention-innovations-and-applications-march-2001/

[39] P. A. Colegrove and H. R. Shercliff, "Development of Trivex friction stir welding tool Part 1 - two-dimensional flow modelling and experimental validation," *Science and Technology of Welding and Joining,* vol. 9, pp. 345-351, Aug 2004.

[40] P. A. Colegrove and H. R. Shercliff, "Two-dimensional CFD modelling of flow round profiled FSW tooling," *Science and Technology of Welding and Joining,* vol. 9, pp. 483-492, 2004 2004.

[41] P. A. Colegrove, H. R. Shercliff, and R. Zettler, "Model for predicting heat generation and temperature in friction stir welding from the material properties," *Science and Technology of Welding and Joining,* vol. 12, pp. 284-297, Jul 2007.

[42] W. M. Thomas, E. D. Nicholas, and S. D. Smith. (2001, 30 Jun 2012). *Friction stir welding - tool developments*. Available: http://www.twi.co.uk/technical-knowledge/published-papers/friction-stir-welding-tool-developments-february-2001/

[43] K. Kimapong and T. Watanabe, "Lap joint of A5083 aluminum alloy and SS400 steel by Friction Stir Welding," *Materials Transactions,* vol. 46, pp. 835-841, Apr 2005.

[44] A. Elrefaey, M. Gouda, M. Takahashi, and K. Ikeuchi, "Characterization of aluminum/steel lap joint by friction stir welding," *Journal of Materials Engineering and Performance,* vol. 14, pp. 10-17, Feb 2005.

[45] K. Kimapong and T. Watanabe, "Effect of welding process parameters on mechanical property of FSW lap joint between aluminum alloy and steel," *Materials Transactions,* vol. 46, pp. 2211-2217, Oct 2005.

[46] A. Abdollah-Zadeh, T. Saeid and B. Sazgari, "Microstructural and mechanical properties of friction stir welded aluminum/copper lap joints," *Journal of Alloys and Compounds*, vol. 460, pp. 535-538, Jul 2008.

[47] F. Vahid and K. Sindo, " Al-to-Cu Friction Stir Lap Welding," *Metallurgical and Materials Transactions A*, vol. 43, pp. 303-315, Jan 2012.

[48] F. M. F. Nascimento, " Processamento por Fricção Linear - Caracterização e Análise das Ligas de Alumínio AA5083-O e AA7022-T6," Mestre em Engenharia Materiais, Universidade Técnica de Lisboa - Instituto Superior Técnico, Nov 2007.

[49] P. Vilaça, T. Santos, PT Patent PT N.º 104072, "Ferramenta Não Consumível Modular Ajustável e Refrigerável para Soldadura e Processamento por Fricção Linear," 2008.

[50] S. M. Chowdhury, D. L. Chen, S. D. Bhole and X. Cao, "Tensile properties of a friction stir welded magnesium alloy: Effect of pin tool thread orientation and weld pitch," *Materials Science and Engineering A*, vol. 527, pp. 6064-6075, Aug 2010.

[51] NP EN 910, “Ensaios Destrutivos de Soldaduras em Materiais Metálicos: Ensaio de Dobragem”, 1996.

[52] R. W. K. Honeycombe, "Aços: microestruturas e propriedades," Fundação Calouste Gulbenkian, Lisboa, 1985.

[53] P. Vilaça, “Fundamentos do Processo de Soldadura por Fricção Linear: Análise Experimental e Modelação Analítica”, PhD Thesis, UTL-IST, 2003.

[54] ASM Handbook Committee, "Metallography and Microstructures," vol. 9, pp. 1850 and 2676, 2004.

Annexes

Annex A – Procedures of FSDP

Preparation phase of the plates to process:

1. Materials selection and procurement.
2. Plate sectioning by guillotine into 200 x 100 mm and 200 x 150 mm copper samples.
3. Plate sectioning by guillotine into 200 x 150 mm stainless steel samples with 1 mm of thickness.
4. Plate sectioning by saw ribbon into 200 x 150 mm stainless steel samples with 6 mm of thickness.
5. Grinding the surface to remove oxides.
6. Air jet on the surface grinded to remove the particles.
7. Clean the surface with alcohol or ethanol.

Procedures used in equipment and processing of the plates:

1. Assemble the tool and setting the probe length.
2. Tool assembly in the machine.
3. Turn on cooling system and verify the water flow.
4. Fixturing system assembly.
5. Put and adjust the plates on the fixturing system.
6. Adjust the fixturing system according to the X-axis of the machine and tighten the fixing.
7. Setting the zero position at the Z axis on the processing plate.
8. Set-up the start and end position of processing at the axes X and Y.
9. Parameters setting into the HMI console.
10. Press "Start" to initiate the rotation of the tool.
11. Press "Start" to begin the FSDP.
12. During the cycle, it was necessary be watchful to process in order to avoid accidents of the tool by pressing the "Stop" button.
13. After the end of the cycle, to unscrew the fixturing system.
14. Remove and mark the joint.

15. Visual inspection and photography of the joint
16. For further processed joints repeat from step 5.
17. At the end of all processing, cleans up and disassemble the tool.
18. Clean up the fixturing system, work table and equipment.
19. Tidy up the accessories used.

Annex B – Metallurgical characterization

Polishing of samples for metallographic analysis were performed according to the following steps:

1. Sample of cross section from surface processed.
2. Mark the sample.
3. Removal of edges shaving and clean the residues.
4. Mark the mould.
5. Lubricate the mold to facilitate the subsequent output of sample
6. Mounting the sample in moulds with the epoxy resin and epoxy hardener.
7. Wait 24 hours for the epoxy resin to harden.
8. Remove the sample from the mould.
9. Clean the mold and sample.
10. Polishing each sample with rotating grinder-polishing machine according to the following sequence: SiC gridding paper 80, 240, 600, 1200 and 2500 lubricated with running water.
11. At the end of each gridding paper, wash, dry and visualize the depth of the scratches on the microscope.
12. Proceed with polishing using a polishing cloth with alumina suspension solution of 1 µm.
13. Wash under running water with the help of cotton to drag the polishing particles and dry the sample.
14. Visualize on the microscope and take photographs of macrograph and micrographs.
15. Etch the copper with reagent prepared according to Table B1.
16. Clean with running water and dry.
17. Visualize on the microscope and take photographs of macrograph and micrographs on the copper side.
18. Etch the austenitic stainless steel with aqua regia reagent prepared according to Table B1.
19. Clean with running water and dry.

20. Visualize on the microscope and take photographs of macrograph and micrographs on the stainless steel side.
21. Merge the macrographs of copper and stainless steel sides.
22. Polishing the sample using SiC gridding paper 2500 lubricated with running water to remove the etch surface.
23. Polishing using a cloth with diamond paste of 3, 1 and 0.25 µm.
24. Keep the sample in a container free of dust and humidity during 24 hours.
25. SEM/EDS analysis and take photographs.

Table B1 – Reagent chemical composition [54].

Reagent	Composition	Etching procedure
Etch of copper	$FeCl_3$ + HCl + H_2O	Swabbing 8 times on the sample
Etch of austenitic stainless steel (Aqua regia)	45 ml HCl (conc) + 15 ml HNO_3 (conc)	Immersion until desired degree of etching

Annex C – Mechanical characterization

Shear test were performed according to the following steps:

1. Cut three samples of the same processing for each parameter, in accordance with standardized dimensions.
2. Mark each sample.
3. Milled edges with a 240 grinding paper to reduce stress concentration points.
4. Measured with a caliper the thickness and width of joint.
5. Tighten the grippers of the machine in the test sample.
6. Measure the distance between the grippers.
7. Set-up the speed test.
8. Initialize the shear test.
9. Stop after rupture of the sample.
10. Save data.
11. Visual analysis.

Procedure for bending test:

1. Cut three samples of the same processing for each parameter, in accordance with standardized dimensions.
2. Mark each sample.
3. Milled edges with a 240 grinding paper to reduce stress concentration points.
4. Set the distance between the rollers.
5. Aligning the center of the sample processing with the center of distance between the rollers.
6. Set-up the speed test.
7. Initialize the bending test.
8. The bending test was interrupted when hit defined offsets for each sample or the machine angular constraints.

9. Save data.

10. Visual analysis and measurement the bending angle.

Annex D – Energy consumption

SCADA files acquired in the production of processed joints were used for the calculation of energy consumption presented in Section 4.4. Tables E1 to E4 summarize information from SCADA files analyzed.

Table D1 – Evolution of energy consumption in type 1 joints for different rotation speeds and constant travel speed of 120 mm/min.

		Sample			
		H 6	H 10	H 18	H 22
Length processed	(mm)	67.0	65.0	65.0	65.0
Time processed	(s)	35.1	34.4	34.3	34.3
T_Z	(N.m)	24.41	21.10	19.07	18.90
Travel speed	(mm/min)	114.5	113.5	113.8	113.8
Rotation speed	(rpm)	1000	1199	1399	1599
Consumption	(W)	2556	2649	2794	3165
	(J)	89699	91140	95844	108559
	(J/mm)	1339	1401	1473	1669

Table D2 – Evolution of energy consumption in type 1 joints for different travel speeds and constant rotation speed of 1400 rpm.

		Sample				
		H 16	H 14	H 18	H 13	H 15
Length processed	(mm)	52.0	65.0	65.0	64.5	64.4
Time	(s)	52.8	45.2	34.3	26.6	22.3
T_z	(N.m)	19.03	19.06	19.07	20.45	20.62
Travel speed	(mm/min)	59.1	86.3	113.8	145.4	173.3
Rotation speed	(rpm)	1399	1399	1399	1399	1399
Consumption	(W)	2788	2793	2794	2996	3021
	(J)	147225	126237	95844	82692	67373
	(J/mm)	2831	1941	1473	1273	1046

Table D3 – Evolution of energy consumption in type 2 joints for different downward forces with constant travel speed of 120 mm/min and rotation speed of 1400 rpm.

		Sample		
		I 16	I 25	I 22
Length processed	(mm)	65.0	64.9	65.0
Time	(s)	66.7	66.5	34.4
T_z	(N.m)	18.46	16.95	18.44
Travel speed	(mm/min)	58.5	58.6	113.5
Rotation speed	(rpm)	1399	1599	1599
Consumption	(W)	2704	2839	3088
	(J)	180381	188791	106232
	(J/mm)	2773	2908	1633

Table D4 – Evolution of energy consumption in type 2 joints for different downward forces with constant travel speed of 120 mm/min and rotation speed of 1400 rpm.

		Sample		
		I 22 C	I 22	I 22 B
Length processed	(mm)	65.0	65.0	65.0
Time	(s)	34.0	34.4	34.0
T_z	(N.m)	17.90	18.44	19.33
Travel speed	(mm/min)	114.7	113.5	114.7
Rotation speed	(rpm)	1599	1599	1599
Downward force	(N)	5000	5500	6000
	(W)	2997	3088	3236
Consumption	(J)	101906	106232	110032
	(J/mm)	1568	1633	1693